A review of linear Fresnel primary optical design methodologies

A.E. Rungasamy, K.J. Craig* and J.P. Meyer

Department of Mechanical and Aeronautical Engineering, University of Pretoria, Pretoria 0002, South Africa.

*Corresponding author: ken.craig@up.ac.za

Highlights

- A review of literature on optical design methodologies of linear Fresnel is given.
- Designing for peak conditions is first considered.
- Using multi-objective optimisation methods is covered in detail.
- Analytical and finite-volume methods to determine optical performance are listed.
- Novel linear Fresnel layouts are critiqued with a discussion of their cost.

Abstract

Linear Fresnel collector plants represent a promising line-focusing concentrating solar thermal technology that has not yet reached commercial maturity. This technology has many advantages, but its core disadvantage is the low optical performance of the primary collector field. The design of the primary is therefore of vital importance to the competitiveness of the technology. The large number of independent parameters in primary collector designs has led to many different optical design methodologies and optimisation studies. This review paper firstly details the different optical loss mechanisms and their relative importance to the performance of the primary. The different models used to quantify performance are then detailed. The subsequent sections categorise the collector primary design into three broad themes: designing for peak conditions (no blocking and shading for a vertical sun); design optimisation (from sensitivity studies to particle swarm and multi-objective optimisation studies); and novel linear Fresnel layouts. Novel layouts make use of additional degrees of freedom and non-imaging optics to create hybridised collector fields with enhanced optical efficiency. While this avenue shows much promise, the cost implications of the added complexity are typically not fully quantified.

Keywords: *linear Fresnel; primary collector; optical design; collector optimisation; optical modelling*

Nomenclature		γ	Geometric intercept factor
A	Azimuth	η_{en}	Energy efficiency
$A_{end\ loss,i,t}$ $A_{blocking,i,t}$ $A_{shading,i,t}$	Fraction of mirror area unused due to different optical loss mechanisms	η_{ex}	Exergetic efficiency
A_m	Mirror area	η_{opt}	Optical efficiency
$A_{x,n}$	Mirror position in x	η_{PV}	Photovoltaic efficiency
C_R	Concentration ratio	η_{sys}	System efficiency
d_R	Receiver displacement	λ	Collector tilt angle
D_w	Distance between mirror centres	ω	Etendue curve angle
f	Mirror focal length	ϕ_n	Mirror targeting angle
G_b	Beam irradiation	ρ	Reflectivity
G_d	Diffuse irradiation		
g_{eff}	Effective beam spread	θ	Surface errors
I	Ray intensity distribution	θ_L	Longitudinal angle
K_{TL}	Incidence angle modifier	θ_{sun}	Sun angle

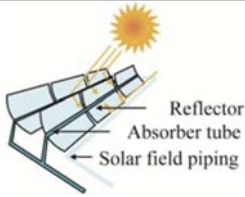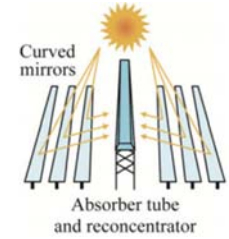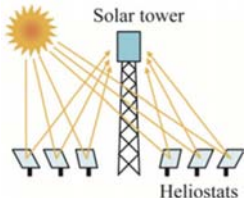|			
K_T	Transversal incidence angle modifier	θ_T	Transversal angle
K_L	Longitudinal incidence angle modifier	θ_i	Incidence angle
L	Length of the collector field	τ	Glass transmissivity
$Q_{field,i,t}$	Energy available to the ith mirror, for time t	σ	Standard deviation of surface errors
$\dot{Q}_{inc}$	Incident radiation on the receiver	μ	Mean value of surface errors
$\dot{Q}_{out,coll}$	Collector power output		
R	Half the focal length of the mirrors	**Abbreviations**	
S_n	Mirror shift	CFD	Computational Fluid Dynamics
T_{amb}	Ambient temperature	CLFR	Compact Linear Fresnel Reflector
T_m	Mean fluid temperature	CPV	Concentrated Photovoltaic
$U_{0,1,2}$	Etendue of incoming (0) or reflected radiation (1,2)	CR	Concentration Ratio
w_n	Mirror width	CSP	Concentrated Solar Power
W_{field}	Field width	DNI	Direct Normal Irradiation
Z	Zenith	IAM	Incidence Angle Modifier
		LCR	Local Concentration Ratio
Greek symbols		LEC/ LCOE	Levelised Cost of Electricity
α	Absorptivity	LFR	Linear Fresnel Reflector
β	Receiver acceptance angle	MCRT	Monte Carlo Ray Tracing

1. Introduction

Fossil fuel-based power plants made up 64.5% of global capacity in 2017 (World Nuclear Association, 2020). Carbon emissions have been directly linked to global warming and climate change (Goodwin *et al.*, 2015), the effects of which represent a threat to human habitat, food security and health (Watts *et al.*, 2020). While fossil fuels were historically a significantly cheaper source of power than their competitors, 56% of all new renewable power plants built in 2019 were cheaper than their fossil fuel counterparts (International Renewable Energy Agency, 2020). Solar power is the form of renewable energy that has experienced the greatest reduction in cost (International Renewable Energy Agency, 2020) and consequently, the largest annual growth in investment in the last three years (International Energy Agency, 2020a).

There are two mechanisms of generating electricity using solar power: the first is by using the photoelectric effect to generate direct current (photovoltaic solar power) and the second is by concentrating solar energy onto a target such that it forms the heat source in a thermoelectric power cycle (concentrated solar power). Advances in photovoltaic technology have made it the cheapest form of electricity production (International Energy Agency, 2020), however the direct generation of electricity means that large scale energy storage remains difficult. Concentrating solar power, by contrast, is readily combined with thermal energy storage (such as molten salt tanks) and can therefore be used to provide stable baseload power. Moreover, these thermal concentrators can be used for a variety of applications in addition to electricity production, such as heating or cooling and the production of industrial process heat (Blanco and Santiago, 2017).

Two categories of concentrating solar power exist: point-focusing and line-focusing solar plants. Line-focusing technologies make up 81% of current CSP capacity worldwide (Al-Kayiem and Mohammad, 2019).The typical operating conditions and layouts of the plants are shown in Table 1 (Sun *et al.,* 2020). Point-focusing plants use dual-axis tracking to concentrate solar radiation onto a single point, while line-focusing plants use single-axis tracking to concentrate solar radiation onto a receiver along a line.

While point-focusing technologies reach higher temperatures (Blanco and Santiago, 2017), the plants are more expensive and more complex (Baharoon *et al.*, 2015). Moreover, point-focusing plants have practical limits in terms of scalability of the solar field; plants above 100MW require very tall towers and heliostats with impractically large distances between them. Line-focusing plants are simply scaled based on their length, allowing their capacity to range from a small-scale rooftop plants providing process heat to a high-capacity power plant hundreds of meters long.

Table 1 Typical operating conditions of different CSP plants (Sun *et al.*, 2020)

			Peak efficiency (%)	Annual efficiency (%)	Operation temperature (°C)	Relative cost	Concentration ratio
Line-focus	Parabolic trough collector (PTC)		20 - 25	14 - 22	250 -550	Low	30 – 80
	Linear Fresnel reflector (LFR)		18 - 20	13 -18	150 - 550	Very low	30 - 80
Point-focus	Central receiver system (CRS)		22 - 24	15 - 23	500 - 1200	High	200 – 1000
	Parabolic dish (PD)		28 - 32	18 - 25	600 - 1500	Very high	1000 - 3000

The two main line-focusing technologies commercially available are parabolic trough collectors (PTC) and Linear Fresnel Collectors/Reflectors (LFC/LFR). Parabolic trough collectors consist of a single, continuous parabolic mirror with a movable tubular receiver while linear Fresnel collectors consist of multiple flat or slightly curved primary mirrors with a fixed receiver. In both cases, the mirrors rotate about the field's longitudinal axis to track the sun throughout the course of the day. Parabolic trough collectors are the most commercially mature concentrating solar technology, representing 72% of the global operational CSP plants (Al-Kayiem and Mohammad, 2019). While parabolic trough collectors report higher optical efficiencies than those of a linear Fresnel collector (Cau and Cocco, 2014; El Gharbi et al., 2011; Häberle et al., 2002; Kincaid et al., 2018; Morin et al., 2012), the plants are significantly more expensive (Desai and Bandyopadhyay, 2015; Giostri *et al.*, 2011; Häberle *et al.*, 2002; Morin *et al.*, 2012; Schenk *et al.*, 2014) and complex to manufacture (Sun *et al*., 2020). In addition, the continuous parabolic mirror causes high wind loads (Zhu *et al.*, 2014), while the receiver

requires flexible joints in order to track the focal point of the mirror.

Table 2 Linear Fresnel power plants (He *et al.*, 2019)

Name	Country	Capacity	Working parameters	HTF	Receiver type	Start date
Solarmundo	Belgium	-	-	Water/steam	Mono	2001
Liddell	Australia	1.0	6.9 MPa, 285 °C	Water	Multi	2004
FRESDEMO	Spain	0.8	11 MPa, 450 °C	Water/steam	Mono	2007
Kimberlina	USA	5.0	4 MPa, 300 °C	Water/steam	Multi	2008
Puerto Errado 1	Spain	1.4	5.5 MPa, 270 °C	Water	Mono	2009
Puerto Errado 2	Spain	30.0	5.5 MPa, 270 °C	Water	Mono	2012
Liddell II	Australia	9.0	5.5 MPa, 270 °C	Water	Multi	2012
Huaneng Nanshan Power Plant	China	1.5	3.5 MPa, > 400 °C	Water/steam	Mono	2012
Augustin Fresnel 1	France	0.25	10 MPa, 300 °C	Water/steam	Mono	2012
Dhursar	India	125	9 MPa, 390 °C	Water/steam	-	2014
eCare project	Morocco	1.0	280 °C	Water	-	2014
Rende-CSP	Italy	1.0	280 °C	Oil	-	2015
Alba Nova 1	France	12.0	5.5 MPa, 300 °C	Water/steam	Mono	2015
Llo plant	France	9.0	7 MPa, 285 °C	Water	-	2015
IRESEN plant	Morocco	1.0	300 °C	Oil	Mono	2016
NTPC Dadri ISCC plant	India	14.0	250 °C	Water	-	2017
Zhaoyang Zhangjiakou CSG Fresnel project	China	50.0	-	Water/steam	-	Dev
Urat Fresnel CSP project	China	50	-	Oil	-	NO
Zhangbei CSG Fresnel project	China	50.0	-	Water/steam	-	NO
Dacheng Dunhuang CSP project	China	50.0	-	Molten salt	Multi	Dev

Linear Fresnel collectors therefore represent a promising line-focusing technology, with a number of advantages. Table 2 lists the linear Fresnel power plants that are currently operational or in development. Because the lower optical performance is the core disadvantage, progression in the optical design of the primary collector becomes vital to the overall competitiveness of the technology. Therefore, the first aim of this review was to determine the factors reducing optical performance, while the second aim was to delineate existing primary LFR collector optical design methodologies. For linear Fresnel models, there are a large number of parameters to consider when designing the collector field, which will enhance the flexibility of the design. These parameters include the individual mirror widths, spacing and number of mirrors as well as whether to allow these mirrors to vary individually or create a uniform condition for all mirrors in the field. At macrolevel, the receiver height, field length and field width also have to be considered because these relate to the total power output from the collector field and the land costs of the plant. These factors create a complex set of design considerations, leading to four broad categories of LFR collector research: designing for peak conditions, design optimisation in the conventional LFR layout and novel linear Fresnel layouts. Where other review papers (Bellos, 2019; Sun *et al.*, 2020; Zhu *et al.*, 2014) give an overview of numerous different aspects of a linear Fresnel plant, this paper critically discusses the principles of the primary mirror field design, due to its outlined importance and the breadth of research on this topic.

2. Optical losses

Due to the large number of independently moving mirrors within a linear Fresnel collector field, adjacent mirrors can interact with one another optically, reducing the amount of radiation that reaches the receiver aperture. In order to reduce these losses, the optical design needs to reduce the optical interaction between different parts of the linear Fresnel collector field. These interactions are geometric in nature and are therefore dependent on the incoming sun conditions relative to the collector field. Fig. 1a (Kalogirou, 2014; Zhu *et al.*, 2014) shows the incoming sun angle, as defined relative to the cardinal directions. The azimuth (A) and zenith (Z) angles, are defined as the projection of the sun angle in the horizontal plane relative to south and the projection of the sun angle in the east-west plane relative to the vertical axis. Alternatively, the sun angle can be defined in terms of its projections in the transversal (θ_T) and longitudinal (θ_L) plane of the primary, as shown in Fig. 1b.
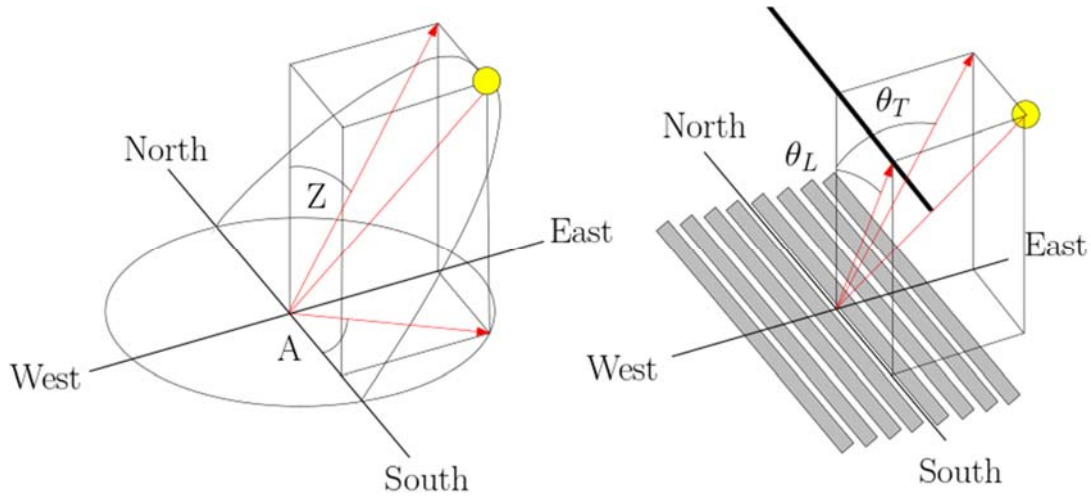

Fig. 1 a) Sun angle relative to cardinal directions and **b)** sun angles for an LFR field (adapted from Kalogirou, 2014; Zhu *et al.*, 2014 respectively)

The longitudinal axis of a linear Fresnel collector is typically aligned in the north-south direction because this increases overall optical performance (Barale *et al.*, 2010) and reduces variation of energy delivery based on the time of day (Feuermann and Gordon, 1991). For a collector aligned about the north-south axis, the transversal angle is calculated as follows:

$$\theta_T = tan^{-1}(sinA \cdot tanZ) \tag{1}$$

while the longitudinal angle is calculated as follows:

$$\theta_L = tan^{-1}(cosA \cdot tanZ) \tag{2}$$

The peak optical efficiency or the optical efficiency for a zenith angle of zero (representing solar noon) is the most significant factor affecting the annual yield of a line-focusing plant, as indicated in Fig. 2 (Eck *et al.*, 2014).
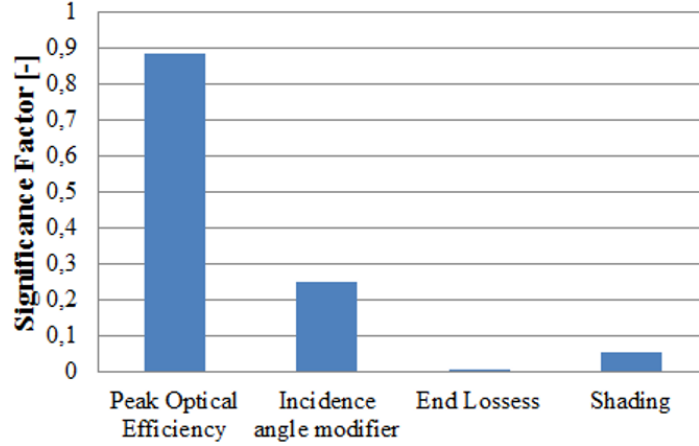
Fig. 2 Significance of the factors affecting optical performance for a line-focusing collector (Eck *et al.*, 2014)

The optical efficiency is defined as the ratio of incident radiation on the receiver ($\dot{Q}_{inc}$) relative to the radiation energy available for a chosen mirror area (A_m) for a given sun angle (θ_{sun}).

$$\eta_{opt}(\theta_{sun}) = 100 \cdot \frac{\dot{Q}_{inc}}{DNI \cdot A_m} \qquad (3)$$

Fossa *et al.* (2021) outlined alternative optical efficiency definitions and demonstrated how the area of reference used within the efficiency definition can substantially affect design and optimisation results. Three optical loss mechanisms affect the peak optical efficiency, namely blocking, shading and missed rays. These are discussed in turn.

1. Blocking: the radiation reflected from a mirror hits another part of the primary mirror field rather than the receiver aperture, as indicated in Fig. 3a (Zhu, 2013).
2. Shading between mirrors: incoming radiation does not reach parts of the mirror field because they are in the shadow of other mirrors, as shown in Fig. 3b (Zhu, 2013).
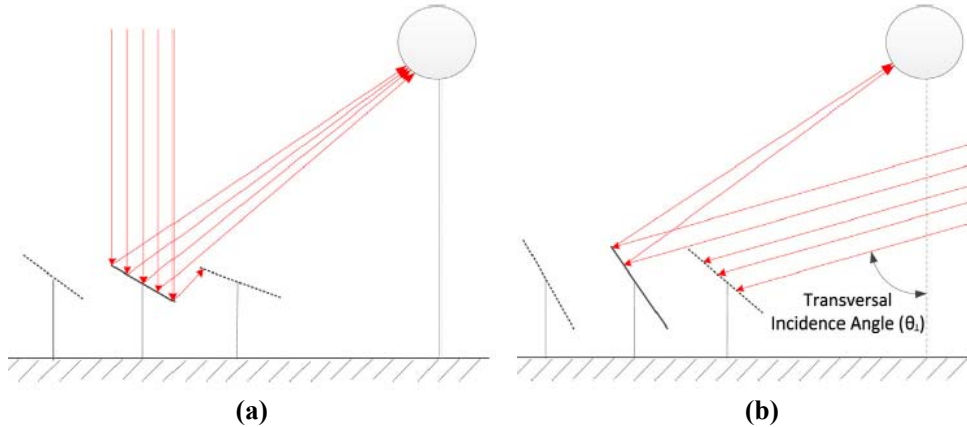

Fig. 3 (a) Blocking and **(b)** shading losses for a linear Fresnel field (Zhu, 2013)

Blocking and shading losses are often considered together in a design, because they are both affected by the gap between mirrors, the transversal distance from the mirror to the receiver and the incoming sun angle. The mirrors farthest from the receiver aperture are most likely to experience blocking (Abbas and Martínez-Val, 2015; Sait *et al.*, 2015) due to fact that the outermost mirrors have similar high targeting angles. As indicated in Fig. 4 (Abbas and Martinez-Val, 2015), shading is less affected by how far the mirror is from the receiver and more affected by the time of day. This is because higher incoming zenith angles lengthen the

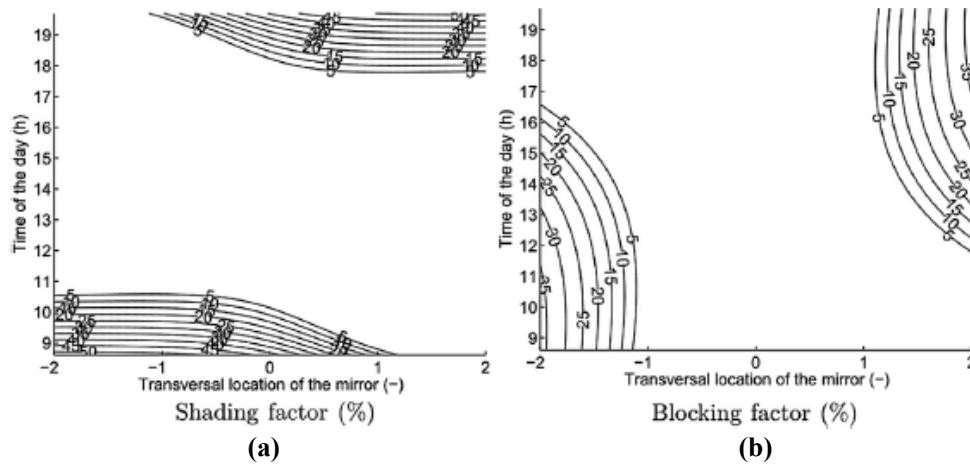shadow of the mirror, causing the shadow to extend beyond the gap and project onto the adjacent mirror.

Fig. 4 Contour of **(a)** shading and **(b)** blocking factors (%) versus time of day and transversal location of the mirror for the *Fresdemo* field in Spain (Abbas and Martínez-Val, 2015)

For very small gaps between mirrors, the blocking and shading losses are very high. Increasing the gap between mirrors can reduce these losses for all but very high sun angles, at which point the DNI (and therefore the amount of available energy) is already low (Sait *et al.*, 2015). However, as this drives up land use and structure costs very large gaps may not necessarily result in the lowest cost of electricity (Morin *et al.*, 2006).

3. Missed rays: a feature of the discontinuous reflective surface of a linear Fresnel primary mirror field is that some rays miss the mirror field entirely, instead hitting the gap between mirrors. However, some optical efficiency definitions account for this effect by calculating the available energy for the given reflector area rather than the aperture area.

While these optical losses occur exclusively within the primary mirror field, incoming radiation can also be prevented from reaching parts of the mirror field due to the shadow cast by the receiver. Eck *et al.* (2014) suggest that receiver shading has a relatively low significance (Fig. 2) because receivers are typically small compared with primary mirror fields. Montenon *et al.* (2019) reported that receiver shading constituted 0.6% of the annual losses for a plant in Nicosia, Cyprus. Nevertheless, when designing the receiver, the shadow it casts on the primary mirror field ought to be incorporated into an integrated optical design consideration.

In addition to the losses occurring within the transversal plane of the primary mirror field, there are also optical losses associated with the longitudinal plane of the plant. Even for peak conditions, plants typically have a non-zero azimuth determined based on its latitude. For this non-zero azimuth, the radiation is reflected up from the mirror through the same angle, resulting in some portion of the rays missing the receiver aperture at the ends (Hongn *et al.*, 2015), as shown in Fig. 5. The end losses are a function of both the latitude of the plant and the length of the primary mirror field. The further the plant is from the equator, the larger azimuth angle, while the longer the primary mirror field is, the smaller the proportion of radiation loss is compared with the total incident radiation on the receiver aperture (Barale *et al.*, 2010; Yang *et al.*, 2018). Sharma *et al.* (2015) suggest that beyond a length-to-width ratio of 1 000, end losses become negligible.
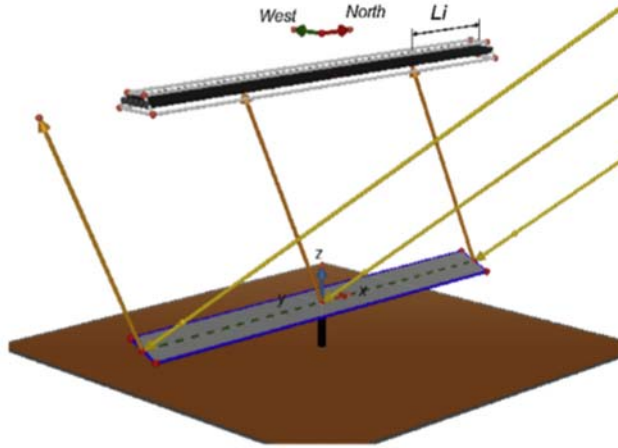
Fig. 5 End losses for an LFR field (Hongn *et al.*, 2015)

While the above losses occur for peak conditions (zero zenith angle, azimuth determined by the latitude of the plant), they increase significantly for off-peak conditions resulting in diminished optical efficiency. This, in addition to the increased attenuation of incoming radiation for larger sun angles (cosine effect), reduces the yield of a primary mirror field. The decrease in efficiency due to the variation of the incoming sun angle is the second most important factor affecting the annual performance of the plant (Eck *et al.*, 2014), as the majority of solar conditions are off-peak conditions. Many studies approximate this decrease in optical performance using the incidence angle modifier (K_{TL}), a ratio which expresses the optical efficiency for a given sun angle (θ_{sun}) relative to the peak optical efficiency ($\eta_{opt,0}$) for a vertical sun, as follows:

$$K_{TL}(\theta) = \frac{\eta_{opt}(\theta_{sun})}{\eta_{opt,0}(\theta_{sun} = 0)} \qquad (4)$$

Because the incoming sun angle (θ_{sun}) consists of different components, McIntire (1982) theorised that the IAM factor for a line-focusing collector could be factorised into its transversal (K_T) and longitudinal (K_L) components, as follows:

$$K_{TL}(\theta_L, \theta_T) \approx K_{TL}(\theta_L, 0) \cdot K_{TL}(0, \theta_T) \approx K_L \cdot K_T \qquad (5)$$

Rönnelid *et al.* (1997) found a 4 to 5% overestimation in annual yield when compared with the full biaxial IAM factor for a CPC collector. Zhu (2013) found a maximum absolute error of 0.05 when comparing the factorised IAM to the coupled IAM function results obtained using the raytracing code (FirstOPTIC) presented within the paper.. Mertins (2009) compared the annual yield obtained through factorised IAM method with simulation based results from two plants, one in Egypt and one in Portugal and found a 2.4% and 3.7% error respectively. However, Horta and Osório (2013) found an average error of 22.67% when comparing the factorised IAM results with ray-tracing results for a 12m long model. The error introduced through the factorisation approach in all of the above cases was one of underestimation, due to a degree of coupling of different loss mechanisms for high zenith and azimuth angles causing asymmetric behaviour as shown in Fig. 6a.
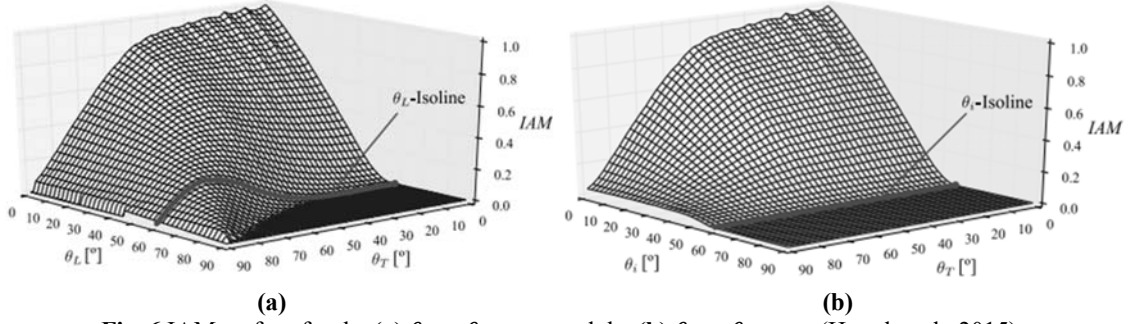
Fig. 6 IAM surface for the **(a)** $\theta_T - \theta_L$ space and the **(b)** $\theta_T - \theta_i$ space (Hertel et al., 2015)

Bernhard *et al.* (2008) suggest that a more accurate IAM factorisation can be obtained by replacing the longitudinal angle with the angle between the sun position vector and transversal plane of the primary mirror field, as follows

$$K_{TL}(\theta_L, \theta_T) \approx K_{TL}(\theta_i, 0) \cdot K_{TL}(0, \theta_T) \approx K_L \cdot K_T \tag{6}$$

With the incidence angle (θ_i) calculated using the azimuth (A) and zenith (Z) angles as follows (Mertins, 2009):

$$\theta_i = tan^{-1}(cosA \cdot sinZ) \tag{7}$$

The use of this alternative definition makes the end losses independent of the transversal angle, effectively decoupling the longitudinal IAM from the transversal IAM, as shown in Fig. 6b. This also means that the cosine effect is better represented (if used within the IAM curve) as

$$cos\theta_{sun} = cos\theta_T \cdot cos\theta_i \tag{8}$$

Holds true by definition (Hertel *et al.*, 2015). Fig. 7 shows the incidence, transversal and longitudinal angles, defined as per equations (7), (1) and (2) respectively
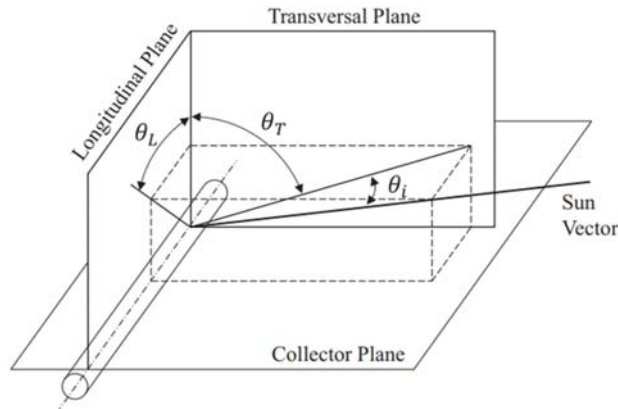

Fig. 7 Incidence, transversal and longitudinal angles (Hertel *et al.*, 2016, 2015; Morin *et al.*, 2012)

Using this factorisation method, Horta and Osório (2013) obtained an average error of 1.65%, which was further reduced to 0.37% when the primary mirror field geometry was extended to 120m. The error in Mertins' (2009) study was reduced to less than 0.5% for both plants. In addition to variation in the choice of angles to use within the factorisation, high and low temperature studies have differed on whether to include the cosine effect within IAM curves (Eck *et al.*, 2014; Morin *et al.*, 2012). If the direct beam radiation on the primary mirror field aperture (G_{bT}) is used, the cosine effect is neglected, however if the Direct Normal Irradiation (DNI) is used, the cosine effect is included. In order to quantify the effects of these differences Hertel *et al.* (2015) presented three latitude dependent annual relative error definitions, whose values are shown in Fig. 8. The inclusion of cosine effects using the incidence

angle (DNI-θ_i) produced the best results, with a small but consistent underestimation of approximately 3%. The use of the longitudinal angle produced relative errors ranging from approximately 10% to 60% regardless of whether or not the cosine effect was included.
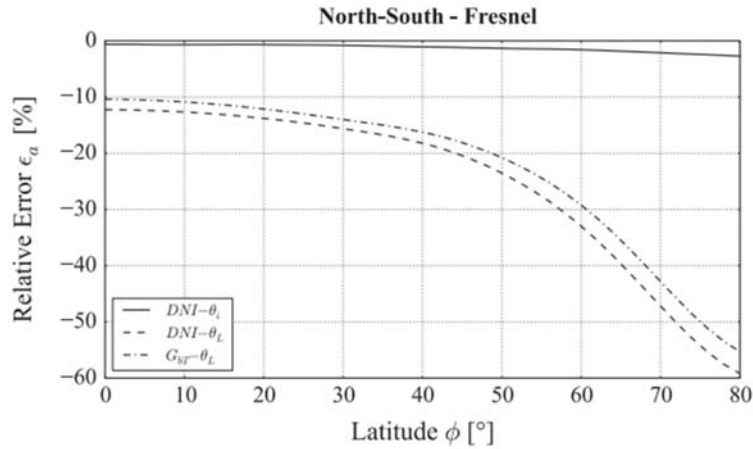

Fig. 8 Annual relative error for different implementations of a factorised IAM (Hertel *et al.*, 2015)

Hertel *et al.* (2016) also investigated whether high process temperatures can affect the accuracy of the IAM factorisation, comparing the annual yield obtained using this approach to the yield obtained using the biaxial IAM. While the error increased for high temperatures, it did not have a significant effect for an economically viable temperature range.

Bellos and Tzivanidis (2018) developed a set of analytical equations to express the transversal and longitudinal IAM in terms of the field parameters and sun angles. The transversal IAM is expressed as a function of the distance between the reflector centres (D_w), the focal length of the mirrors (*f*), the mirror width (w_m), the field width (W_{field}), the mean value of the mirror angles ($\phi_{n,mean}$) and the transversal solar angle (θ_T)

$$K_T(\theta_T) = \begin{cases} \cos\left(\dfrac{\theta_T}{2}\right) - \dfrac{W/4}{f + \sqrt{f^2 + \left(W/4\right)^2}} \sin\left(\dfrac{\theta_T}{2}\right), & \theta_T < \theta_{T,crit} \\[4ex] \left[\cos\left(\dfrac{\theta_T}{2}\right) - \dfrac{W/4}{f + \sqrt{f^2 + \left(W/4\right)^2}} \sin\left(\dfrac{\theta_T}{2}\right)\right] \cdot \left[\dfrac{D_w}{w_m} \cdot \dfrac{\cos(\theta_T)}{\cos\left(\dfrac{\theta_T + \phi_m}{2}\right)}\right], & \theta_T \geq \theta_{T,crit} \end{cases} \qquad (9)$$

While the longitudinal IAM is a function of focal length of the mirrors (*f*), the length of the primary mirror field (L), the field width (W_{field}) and the longitudinal solar angle (θ_L)

$$K_L(\theta_L) = \cos(\theta_L) - \frac{f}{L} \cdot \sqrt{1 + \left(\frac{W_{field}}{4 \cdot f}\right)^2} \cdot \sin(\theta_L) \qquad (10)$$

These expressions were compared to three plants from literature and three commercial plants. The maximum mean deviation for the transversal IAM was 5.43%, while the maximum mean deviation for the longitudinal IAM was 4.8%. This is a relatively high level of accuracy, which could potentially be further improved with the use of the incident solar angle within the model. The optical losses detailed above and their effect on the optical performance of the primary mirror field are typically assessed using one of three performance models; a Monte Carlo Ray Tracing (MCRT) model, an analytical model or a finite volume model.

3. Optical performance modelling

3.1 Monte Carlo ray tracing

The majority of optical performance studies are completed with Monte Carlo Ray Tracing (MCRT) simulations, using either commercial software such as SPRAY (Osório *et al.*, 2016) and HFLCAL (Bode and Gauché, 2012); or publicly available software such as SolTrace (Wendelin *et al.*, 2013), Tonatiuh (Blanco *et al.*, 2011), OTSun (Cardona and Pujol-Nadal, 2020) and Tracer (Y. Wang *et al.*, 2020). Three aspects affect the accuracy of the solution; the number of rays, the modelling of the solar source and the modelling of the optical properties. MCRT programs are stochastic in nature, generating a specified number of rays randomly or pseudo-randomly from a source (Fan *et al.*, 2018). Increasing the number of rays therefore increases both the accuracy and computational time of the simulation (Wang and Zhou, 2019). In early research efforts, the number of rays was largely dictated by the computing capacity available, however, with advances in both computing and MCRT software, the maximum allowable number of rays has increased exponentially. Thus, ray independence studies are typically performed to determine the appropriate number of rays required to represent a statistically meaningful sample (Modest, 2013).

The second aspect of MCRT modelling pertains to the modelling of the solar source. For clear sky conditions, the direction and intensity of the incoming solar radiation is dictated by the solar geometry, time of year/day and the location of the plant. The sun shape, however, is dictated by the portion of energy transferred from the solar disk to the circumsolar aureole due to the interaction of the incoming radiation with particles in the atmosphere (Buie and Monger, 2004). While some models simplify the sun shape to collimated light, sun shape modelling alone can lead to a 20% difference in optical performance (Buie *et al.*, 2003) and significantly affects the flux distribution on receiver apertures (Bendt *et al.*, 1979). MCRT programs therefore typically have built in typical sun shape profiles such as Pillbox, Gaussian and Buie, and/or the capacity to enter user defined profiles (Osório *et al.*, 2016). The pillbox shape neglects all circumsolar radiation and assumes a uniform radiation profile within the solar disk, while the Gaussian profile assumes a Gaussian distribution across the entirety of the solar disk and circumsolar aureole. Rabl and Bendt (1982) found that the Gaussian sun shape consistently underestimated the radiation reaching the receiver for any practical concentration value, while Schubnell (1992) found that a pillbox sun shape resulted in a 5% overestimation of the conversion efficiency of a solar furnace and parabolic concentrator. Wang *et al.* (2020) details the optical modelling of the sun shape and surface slope error for six MCRT programs, evaluating the difference in recorded energy and flux profiles for a variety of cases. The final consideration with regards to sun shape is its link to the intensity of the solar radiation; Neumann *et al.* (2002) found that different DNI ranges corresponded to different proportions of the radiant flux being transferred to the circumsolar aureole (defined as the circumsolar ratio CSR). The probability of typical circumsolar ratio ranges occurring for different DNI ranges is listed in Table 3.

Table 3 Probability of circumsolar profiles occuring for different DNI ranges (Neumann *et al.*, 2002)

CSR Bin, %	Frequency in DNI Bin, %					
	DNI Bin, W/m^2					
	0-200	200-400	400-600	600-800	800-1000	1000-1200
0-4	5.7	19.3	47.5	77.4	74.1	100.0
4-7	0.0	6.8	9.3	12.4	22.8	0.0
7-15	0.0	9.3	20.3	7.4	3.0	0.0
15-25	2.9	21.1	18.3	2.7	0.1	0.0
25-35	5.7	26.1	4.1	0.1	0.0	0.0
>35	85.7	17.4	0.6	0.0	0.0	0.0
Sum	100	100	100	100	100	100

The final aspect of importance in MCRT modelling is the optical properties used within the system, as this dictates the degree of reflection, absorption and transmission occurring on a surface. Different MCRT programs use different implementation strategies to model these optical interactions; the details of which can be found in papers by Liu *et al.* (2020), Wang *et al.* (2018) and Mahan (2019). Optical properties can vary angularly, thermally and based on the wavelength of the light hitting the surface. While MCRT models typically do not incorporate thermal and wavelength based variations of optical properties directly, provision is made within a number of programs to incorporate angular variations in optical properties (Cardona and Pujol-Nadal, 2020; Cardoso *et al.*, 2018; Wendelin *et al.*, 2013). In addition, surface errors (slope, specularity, tracking and alignment errors) affect the optical interactions within the domain. The total surface error (θ_{total}) is defined as the sum of these individual errors, with the slope error multiplied by two due to Snell's law (Osório *et al.*, 2016)

$$\theta_{total} = 2\theta_{slope} + \theta_{specularity} + \theta_{track} + \theta_{align} \quad\quad\quad (11)$$

Most programs do not include the full definition of these surface errors; focussing on slope and specularity or simply the scope error. These errors are typically modelled as pillbox or Gaussian distributions, the effect of which is investigated by Wang *et al.* (2020, 2018).

In addition to an array of ray tracing programs, supplementary programs have been developed to assist with postprocessing (Blanco *et al.*, 2019) and geometry visualisation within a Computer Aided Design (CAD) environment (Cardona and Pujol-Nadal, 2020; Cardoso *et al.*, 2018). The maturity, accuracy and adaptability of the Monte Carlo Ray Tracing methodology have therefore made it the most widely used modelling tool in optical design and performance assessment for CSP applications. The papers subsequently detailed within sections 4 - 6 thus use MCRT programs to assess the optical performance of the primary mirror field unless otherwise specified.

3.2 Analytical models

While analytical models may become complex due to the optical interactions of a large number of discrete mirrors, they are typically faster than MCRT simulations and are thus particularly useful when a large number of simulations must be run, as is the case in annual optical performance assessments. Moreover, they provide an ability to examine individual loss contributions in detail, which can provide greater insight into the main contributors to the optical losses of a specific primary mirror field configuration (Sharma et al., 2015a) The directional nature of beam radiation allows for the optical interactions in the primary mirror field to be modelled geometrically. These interactions are governed by the modelling of the incoming solar radiation, broadly categorised as either parallel beam models or beam spread models.

Models that assume all incoming beam radiation as parallel can consequently use the edge-ray principle (Ries and Rabl, 1994) to calculate the part of the aperture that is unused due to end losses (Hongn *et al.*, 2015) and blocking and shading losses (Pino et al., 2013; Sharma et al., 2015a). The ratio between the lost aperture area and total mirror aperture area is equivalent to the ratio between the radiation losses and the incident radiation on the mirror for the specified instant. Therefore, the calculation can be used to determine the radiation losses of each mirror. As with optical losses, aperture area loss is a function of both the primary mirror field geometry and the incoming solar geometry at any instant. Sharma *et al.* (2015a) derived equations for the instantaneous unused length and width due to blocking, shading and end losses by creating multiple cases of trigonometric equations with associated bounding solar angles.

Once the instantaneous aperture loss is calculated, the available energy for the ith mirror can be calculated based on the fraction of the aperture remaining after the aperture end loss ($A_{end\ loss}$), blocking ($A_{blocking}$) and shading ($A_{shading}$) reductions have been factored in(Sharma et al., 2015a):

$$Q_{avail,i,t} = Q_{field,i,t} \left(1 - \frac{A_{end\ loss,i,t}}{A_{total,i,t}} - \frac{A_{shading,i,t}}{A_{total,i,t}} - \frac{A_{blocking,i,t}}{A_{total,i,t}} \right) \quad\quad (12)$$

Note that the incident radiation on the primary mirror field aperture at a given time ($Q_{field,i,t}$) incorporates cosine effects into its definition as follows

$$Q_{field,i,t} = w_m \cdot L \cdot I_{bn,t} \cdot cos\theta_{i,t} \tag{13}$$

The total available energy from the primary mirror field over a period of time is then expressed as the sum of the available energy from each mirror ($E_{avail,i,t}$) integrated with respect to the time period of interest:

$$Q_{avail} = \int_{t1}^{t2} \left[\sum_{i=1}^{n} Q_{avail,i,t} \right] dt \tag{14}$$

In addition to the modelling of optical losses, a thermal loss and Levelised Cost of Electricity (LCOE) model was proposed within the study. The model was compared to simulation results for the *Fresdemo* LFR plant using solar resource data from Daggett, USA (Morin *et al.*, 2012). Using this model, Sharma *et al.* (2015a) reported the effect of orientation, location and pitch/receiver height to reflector aperture ratio on the annual performance and resultant LCOE. The optical losses for a standard Linear Fresnel Reflector, Parabolic Trough Collector and Compact Linear Fresnel Reflector were derived using this model (Sharma *et al.*, 2015b). Beltagy *et al.* (2017) incorporated loss factors into the calculation of the power reflected onto the receiving tube by performing successive reductions on the power received by the field. While it is unclear how these loss factors were derived, the model was validated against an experimental setup in Seyne, France

Hongn *et al.* (2015) employed a similar methodology to derive a model for end losses, using instantaneous non-illuminated lengths integrated over the time period of interest. The end losses obtained from this model were validated against a North-South aligned LFR prototype in Salta, Argentina and are of particular interest for rooftop LFR installations. An alternative to calculating the non-illuminated fraction of the receiver length and subtracting it from the total length is to calculate the illuminated fraction of the receiver length (Heimsath *et al.*, 2014). Barbón *et al.* (2016) adapted the expression for the illuminated length of the receiver and the equations for blocking and shading by Sharma *et al.* (2015a) to the transversal and longitudinal design of a small scale LFR model. The longitudinal design was used to optimize the receiver tube position and length (Barbón *et al.*, 2016b) and to determine the influence of different longitudinal tilt angles (Barbón *et al.*, 2019) for the same small scale experimental prototype in Asturias, Spain. Within these studies, Barbón *et al.* (2019, 2016a, 2016b) made an assumption of parallel light and did not incorporate optical errors into the analytical model proposed. A subsequent study investigated the effect of the solar tracking error on the absorbed power for a monotube receiver with a secondary (Barbón *et al.*, 2020).

Models that account for beam spread typically assign a probability distribution across the solid angle of the beam (Huang *et al.*, 2014; Zhu, 2013). The overall probability distribution consists of a number of Gaussian distributions (Bendt *et al.*, 1979) representing the sun shape, specularity errors, slope errors, receiver position errors and tracking errors. The mean (μ) and standard deviation (σ) values of the total distribution for the effective beam spread are defined as follows:

$$\mu_{total} = \mu_{sun} + \mu_{specularity} + 2\mu_{slope} + \mu_{receiver} + 2\mu_{track} \tag{15}$$

$$\sigma_{total}^2 = \sigma_{sun}^2 + \sigma_{specularity}^2 + \left(2\sigma_{slope}\right)^2 + \sigma_{receiver}^2 + (2\sigma_{track})^2 \tag{16}$$

Because this distribution is centred around the solar beam, the beam directional vectors can be derived and used to calculate the limits of the receiver acceptance angle (β). Blocking and shading are treated as geometric modifications to the primary mirror field and are subsequently incorporated into the calculation of the modified limits of the receiver acceptance angle. Huang *et al.* (2014) provide a simplified approximation of the blocking and shading modification, while Zhu (2013) uses a complex

series of vector operations. The local intercept factor is then calculated as the integrand of the effective beam spread (g_{eff}) over the modified receiver acceptance angles (β):

$$\gamma^{k,local}(x,z) = \int_{\beta_{3D}^{-k}(x,z)}^{\beta_{3D}^{+k}(x,z)} g_{eff}(\beta)\, d\beta \qquad (17)$$

The mirror intercept factor (γ) incorporates the cosine losses of each mirror into its definition, such that the total intercept factor is simply defined as the sum of the mirror intercept factors. This total intercept factor is used to calculate the optical efficiency of the field (Bendt *et al.*, 1979) along with the mirror reflectivity (ρ), glass transmissivity (τ) and receiver absorptivity (α) as follows:

$$\eta = \gamma \rho \tau \alpha \qquad (18)$$

Lastly, there are semi-analytical optical models such as the adaptation of ISO 9806:2013 guidelines (Hofer *et al.*, 2015) to calculate annual optical efficiency. This adaptation uses an iterative multiple linear regression to solve for the transversal (K_T) and longitudinal (K_L) incidence angle modifiers. The beam irradiation (G_b), diffuse irradiation (G_d), mean fluid temperature (T_m) and the collector power output ($\dot{Q}_{out.col}$) are measured experimentally (in this case using a small-scale LFR in Freiburg, Germany). The measured values are used to solve for the transversal (K_T) and longitudinal (K_L) incidence angle modifiers, according to the following equation

$$\frac{\dot{Q}_{out.col}}{A_{ap}} = \eta_{opt,0} \cdot K_T(\theta_T) \cdot K_L(\theta_L) \cdot G_b + \eta_{opt,0} \cdot K_d \cdot G_d - c_1 \cdot (T_m - T_{amb}) - c_2 \qquad (19)$$

$$\cdot (T_m - T_{amb})^2 - c_5 \frac{dT_m}{dt}$$

With c the coefficients of the equation. The second semi-analytical model proposed is one in which the measured values are used to optimise the transversal (K_T) and longitudinal (K_L) incidence angle modifiers within an in-house simulation model (ColSim).

3.3 Finite volume models

Many studies use the ray data obtained from MCRT simulations to generate a nonuniform flux profile that is applied to the absorber tube surface(s) within a Computational Fluid Dynamics (CFD) environment, as shown for both a monotube and multitube receiver in Fig. 9.
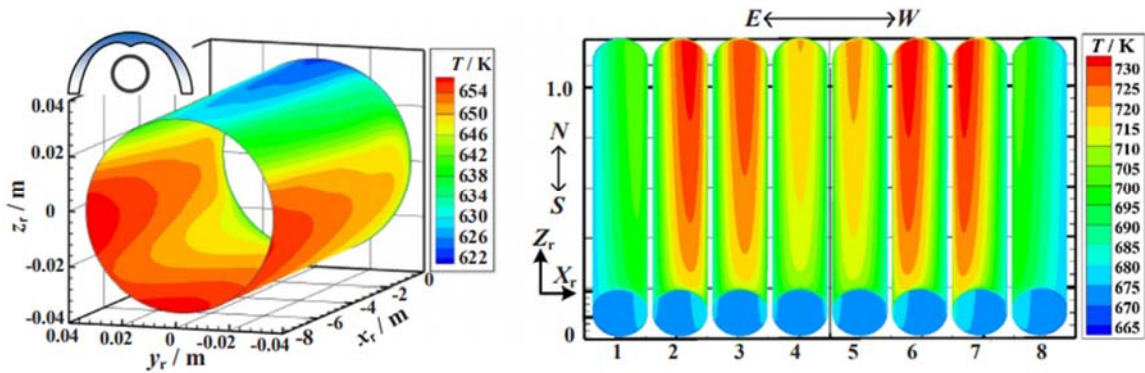

Fig. 9 Non-uniform temperature distributions for a monotube (left) and multitube receiver (right) (Li *et al.*, 2019; Qiu *et al.*, 2016, 2015)

However, an alternative to this is to model the optics directly within the CFD environment, using a finite volume optical model. While both analytical and MCRT models are faster, finite volume modelling offers the opportunity to model more complex interactions such as non-grey radiation and spectrally or thermally dependent material properties (Coelho, 2014). Moreover, the CFD environment

facilitates design optimisation through a number of built-in optimisation strategies, which can be done on both a thermal and optical basis when the two forms of analysis are integrated into one platform. Many radiation models exist in commercial CFD solvers, with the discrete ordinates (DO) method the most accurate for modelling complex radiation interactions (Miller and Reed, 1977). The memory requirements for finite volume modelling are modest when considering a low number of angular discretisations, but for fine angular discretisation, the simulation may be memory and CPU intensive (Coelho, 2014). They are also relatively accurate, but the core disadvantage of this type of model is the propagation of two types of errors: false scattering and ray effect (Chai *et al.*, 1993). False scattering or numerical diffusion is a dissipative error that smooths out sharp discontinuities and large gradients. It is caused by a truncation error when approximating the governing partial differential equations as discrete terms using finite-differencing schemes (Hunter and Guo, 2015). Therefore, this error depends on the spatial discretisation of the domain (Li, 2004). The lowest-order term in the truncation error dominates the behaviour of the numerical scheme: if it is an even derivative, the error is dissipative; if odd, the error is dispersive (Chai *et al.*, 1993).

Ray effect is caused by approximating the continuously varying angular nature of radiation as a set of discrete angular directions (Chai *et al.*, 1993; Craig *et al.*, 2016; Raithby, 1999). Therefore, it is directly affected by the resolution of the angular discretisation. The effect of this error is a distortion of the heat flux distribution and a displacement of the peaks of the solution (Craig *et al.*, 2016). While early studies theorised that false scattering was completely independent of ray effects, it was later found that the two are not independent and in fact have compensatory effects (Chai *et al.*, 1993; Coelho, 2014, 2002; Hunter and Guo, 2015; Raithby, 1999).
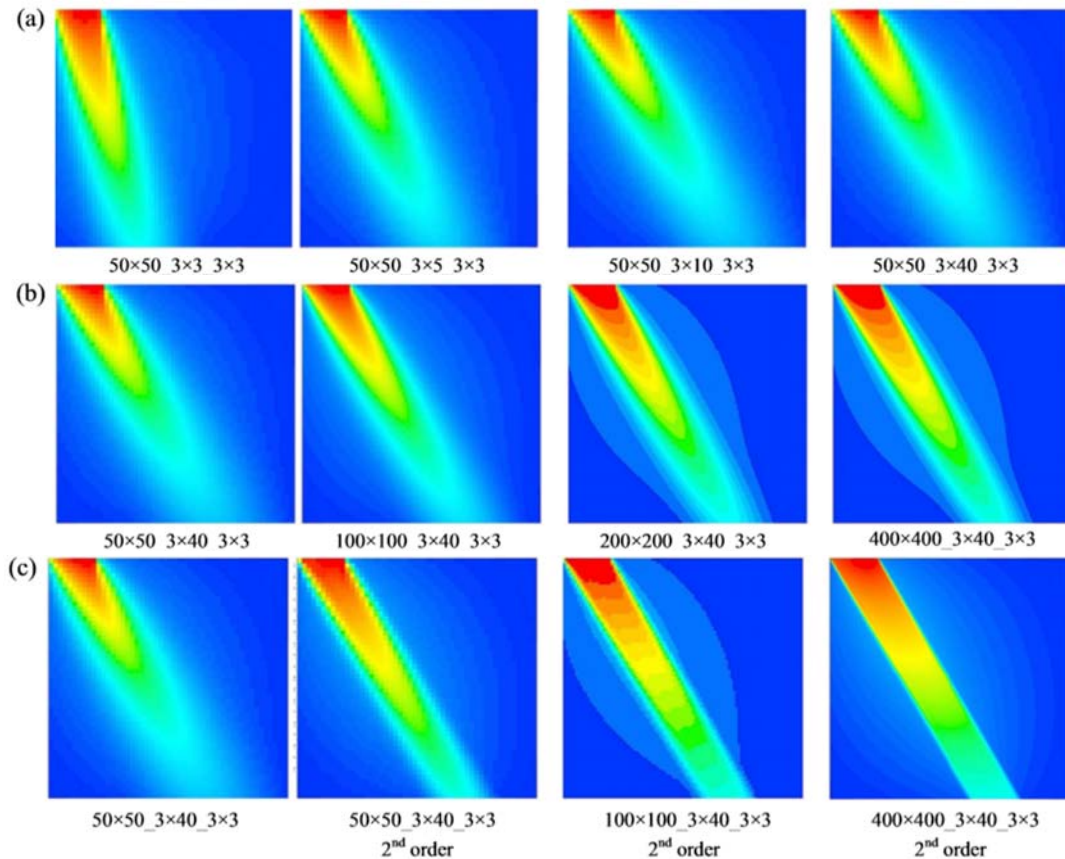

Fig. 10 CFD DO solution for oblique collimated light for a variety of mesh (meshX × meshY) and control angle refinements (_phi × theta) (Craig *et al.*, 2016)

In order to reduce the errors associated with ray effects and false scattering, a sufficiently refined spatial mesh and control angle count must be used (Craig *et al.*, 2016; Hunter and Guo, 2015; Moghimi *et al.*, 2015). Mesh and control angle sensitivity studies must be completed and the solution compared with either an MCRT solution in a code-to-code comparison, or physical results from testing. Fig. 10 (Craig *et al.*, 2016) shows the effects of increasing the spatial mesh and control angle count for a simple simulation of collimated light.

At the low control angle counts in Fig. 10a, the collimated light is both directionally distorted and dissipated through the domain. While increasing the control angle count independently (Fig. 10a) does correct the directional distortion within the solution, the dissipative error isn't affected. The solution is further refined by increasing the spatial mesh count (Fig. 10b), which reduces the dissipative error to a degree. Thus, the combination of the control angle refinement, mesh refinement and higher order discrete ordinations equations must be used in order to model the collimated light in a realistic way (Fig. 10c). Using the appropriate settings, good correlations with MCRT results can be obtained for a variety of CSP geometries (Craig *et al.*, 2016; Moghimi, 2017; Moghimi *et al.*, 2016, 2015; Rungasamy, 2020).

López-Núñez *et al.* (2020) used ANSYS Fluent to assess the energy and entropy generation of a linear Fresnel prototype in Morelos, Mexico. The finite volume model was compared to experimental data, resulting in a maximum relative error of 2.36% for the energy efficiency, 5.15% for the exergy efficiency and 2.23% for the outlet temperature. Fig. 11 shows the resultant radiation and temperature contours for the full field and receiver respectively.
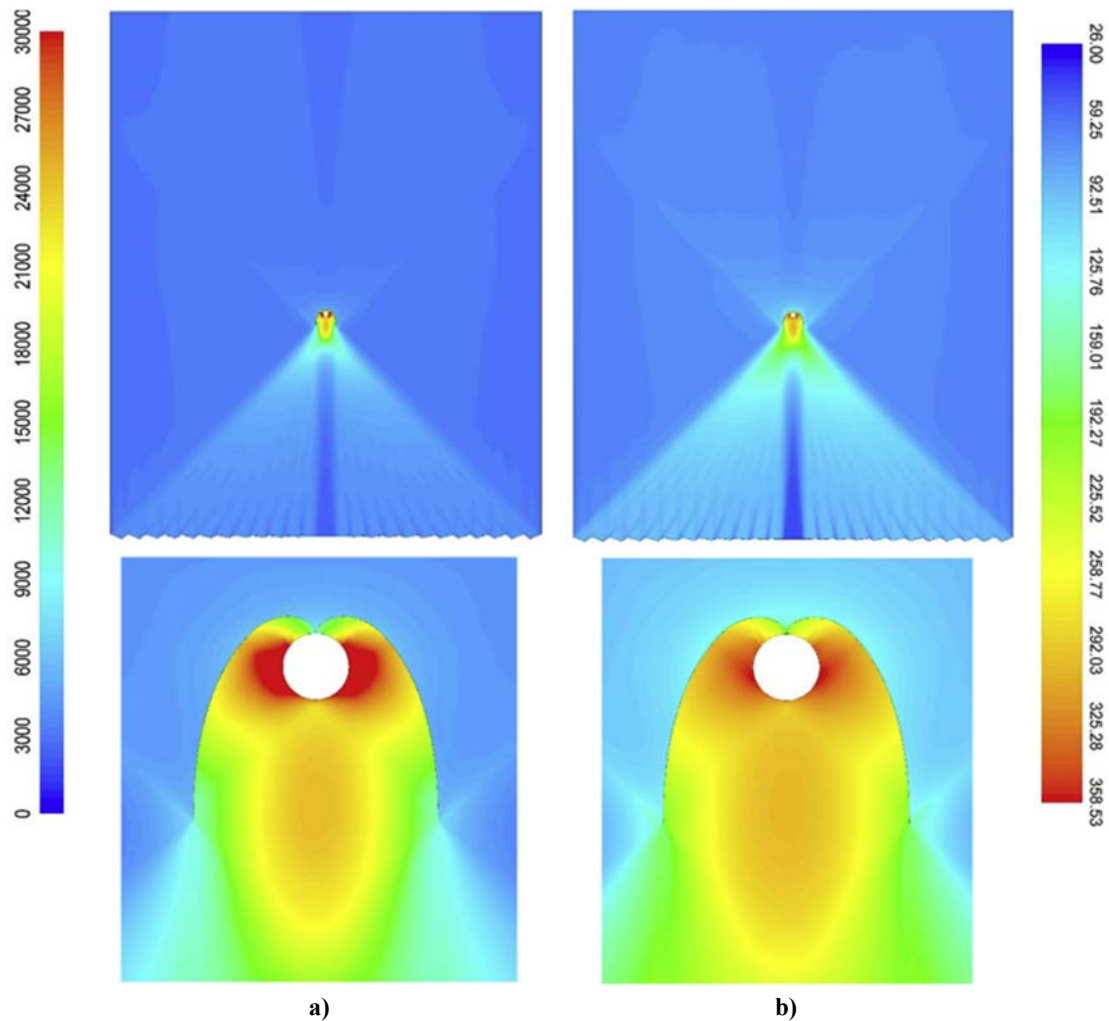

Fig. 11 Contour of **(a)** incident radiation (W/m^2) and **(b)** radiation temperature (°C) (López-Núñez *et al.*, 2020a)

This model was subsequently used to optimize the linear Fresnel reflector, using the Evolutionary Programming method in order to maximise the absorbed radiation on the absorber tube and minimise the entropy generation rate (López-Núñez *et al.*, 2020b). The optimum design increased the absorbed radiation by 2.48% and decreased the entropy generation rate by 20%, resulting in a thermal efficiency of $\eta_{en} = 0.28$ and an exergy efficiency of $\eta_{ex} = 0.047$.

4. Designing for peak conditions

Early optical designs of linear Fresnel mirror fields investigated the use of both equal and variable width mirror fields and reported the concentration ratios for different absorber configurations, as well as the validity of some of the simplifying assumptions made. The earliest designs (Singh *et al.*, 1980; Singhal *et al.*, 1982) of linear Fresnel fields were based on a vertical sun condition, allowing the mirror widths to vary such that the reflected radiation from each mirror covered the entirety of the absorber aperture. This was done because the LFR field was originally conceived as a way to enhance the performance of photovoltaic cells. The mirrors were positioned in order to meet the condition that no blocking and shading occurred between mirrors for the incoming vertical sun. Because there was a negligible shadow, the first mirror was placed at a distance equal to half of the receiver aperture and the other mirrors' position ($A_{x,n}$), width (w_n) and targeting angles (ϕ_n) were determined iteratively using the mirror gap/shift (S_n), the aperture width (W_A) and the receiver height (H_R) in terms of Eqs. (20) to (23):

$$A_{x,n} = A_{x,n-1} + S_n + w_{n-1} \cdot cos\phi_{n-1} \tag{20}$$

$$\phi_n = \frac{1}{2} \cdot arctan\left(\frac{A_{x,n}}{H - \frac{W_A}{2}}\right) \tag{21}$$

$$w_n = 2W_A \cdot sin\phi_n \tag{22}$$

$$S_n = \frac{(A_{x,n-1} + w_{n-1} + cos\phi_{n-1}) \cdot w_{n-1} \cdot sin\phi_{n-1}}{\left(H_R - \frac{W_A}{2}\right) - w_{n-1}} \tag{23}$$

As the temperature increase within the heat transfer fluid is a consequence of the concentration of solar radiation, the concentration ratio (C_R) is an important parameter affecting the efficiency of the primary mirror field. This ratio is defined as the irradiance on the receiver surface (I_{rec}) relative to the incident solar irradiation on the mirror aperture (I_m) (Lovegrove and Stein, 2020)

$$C_R = \frac{I_{rec}}{I_m} = \frac{I_{rec}}{DNI} \tag{24}$$

The Local Concentration Ratio (LCR) indicates the concentration ratio (C_R) for a specified position in the receiver. Both studies reported concentration ratios of approximately $C_R = 6.8$. Singhal *et al.* (1986) subsequently reported concentration ratios of approximately $C_R = 14$ through experimental results for a field designed to obtain a local concentration ratio of $C_R = 28$. While variable mirror widths have the advantage of creating an even profile across the receiver aperture, it also increases the manufacturing complexity. Negi *et al.* (1990) compared the local concentration ratios of a field with variable mirror widths with a field with equal mirror widths using the same design technique to position the mirrors. The resultant LCR profiles were obtained analytically and through the use of ray tracing, as shown in Fig. 12a and b.
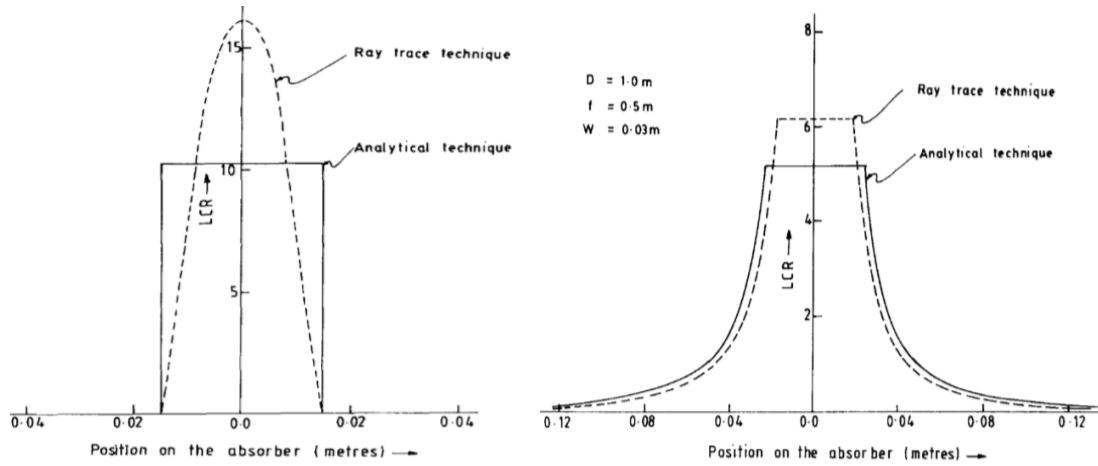
Fig. 12 Distribution of Local Concentration Ratio (LCR) on both surfaces of a flat vertical absorber for **(a)**

variable width mirrors and **(b)** equal width mirrors (Negi et al., 1990)

The variable mirror width design in Fig. 12a has a higher concentration across the width of the receiver aperture, while the equal mirror width design in Fig. 12b has a much wider concentration distribution with a lower peak. A second feature of the two concentration distributions is the difference between the ray-tracing and analytical techniques. This is attributed to the fact that the reflected radiation from each mirror is assumed to be evenly distributed across the width of the aperture (Negi *et al.*, 1990; Singh *et al.*, 1980; Singhal *et al.*, 1986). An experimental setup by Negi *et al.* (1989), consisting of mirrors of an equal width of $w = 0.025$m and three different tubular receivers reported optical efficiencies of $\eta_{opt} = 36$ - 57%. The low optical efficiencies were attributed to poor mirror reflectivity and inaccurate tracking.

The technique of placing mirrors such that no blocking and shading occur for a vertical sun angle was subsequently used with different absorbers to further characterise the local concentration profiles of the primary mirror field. Goswami *et al.* (1990) investigated the variable and equal mirror width designs for a triangular absorber, obtaining a maximum ray trace based concentration ratio of $C_R = 34$ for a receiver with each side at 20° to the vertical axis. The maximum concentration ratio decreased as the angle to the vertical increased. Mathur et al. considered the variable (Mathur *et al.*, 1991a) and equal (Mathur *et al.*, 1991b) mirror width designs for a flat vertical absorber, a flat horizontal absorber and a single-tube absorber. The maximum ray trace based concentration ratio reported for the variable mirror width were $C_R = 16$, $C_R = 37$ and $C_R = 29$ for the respective receivers. For the equal mirror width study, the maximum ray trace based concentration ratios for the same three receivers were $C_R = 6.2$, $C_R = 25$ and $C_R = 25$. In all cases, the first mirror was placed just beyond the shadow of the receiver because different absorber shapes would cause shadowing. The studies produced similar results in terms of LCR distributions as well as in terms of the difference between analytical and ray-tracing techniques.

The consistent differences found between the local concentration profiles obtained through the analytical technique and the ray-tracing technique (Goswami *et al.*, 1990; S. S. Mathur *et al.*, 1991; S.S. Mathur *et al.*, 1991; Negi *et al.*, 1990; Singh *et al.*, 1980) call into question the validity of the assumption that radiation is evenly distributed across the solar disk and across the width of the aperture. Sootha and Negi (1994) investigated this assumption for the equal mirror field design, comparing an equal distribution across the solar disk with a distribution that decreased with distance across the solar disk. A weight was assigned to the rays across the solar disk using the method proposed by Negi *et al.* (1985), in order to obtain the following correlation (Evans, 1977):

$$0.785 \cdot I_{constant\ intensity\ disk} = 0.625 \cdot I_{non-uniform\ disk} \hspace{2cm} (\ 25\ )$$

The form of the distributions of the local concentration ratios around the absorber tube using a constant intensity across the solar disk matched those obtained by Mathur *et al.* (1991a,1991b) for a tubular absorber using the ray-tracing technique. However, the non-uniform intensity across the solar disk changed the local concentration ratio profile significantly, specifically increasing the peak LCR obtained. Therefore, the intensity distribution across the solar disk is an important consideration in the optical design of a linear Fresnel primary mirror field. Additionally Sootha and Negi (1994) found that sizing the mirror width based on a given absorber size resulted in higher LCRs than sizing the absorber based on the mirror width.

The first commercial plant (the *Solarmundo* project) began construction in Liège, Belgium in 1999 (Häberle *et al.*, 2000). The direct steam plant, consisting of a monotube receiver with a compound parabolic secondary, reported a peak optical efficiency of $\eta_{opt} = 63\%$. The project also provided the first costing information for commercial linear Fresnel plants, which was used to create a costing model for standard linear Fresnel collectors (Mertins, 2009). The collector costs within this model were grouped into those associated with the primary mirror, the receiver, the structure associated with mounting the receiver and the additional structure between mirrors. These costs were expressed as coefficients, normalised on a per metre or per square metre basis and thus could be generalised for other layouts.

A prototype Compact Linear Fresnel Reflector (CLFR) plant, that alternates between two receivers (section 6.1), began construction in 2003 in New South Wales, Australia (Pye *et al.*, 2003). The plant consisted of multitube receivers and made use of parabolic mirrors instead of flat mirrors. Curving the mirrors reduces the width of the reflected radiation profile by creating a focal point for the rays, as shown in Fig. 13. This in turn means that wider mirrors can be used for the same receiver aperture width without causing spillage (Pulido *et al.*, 2017).
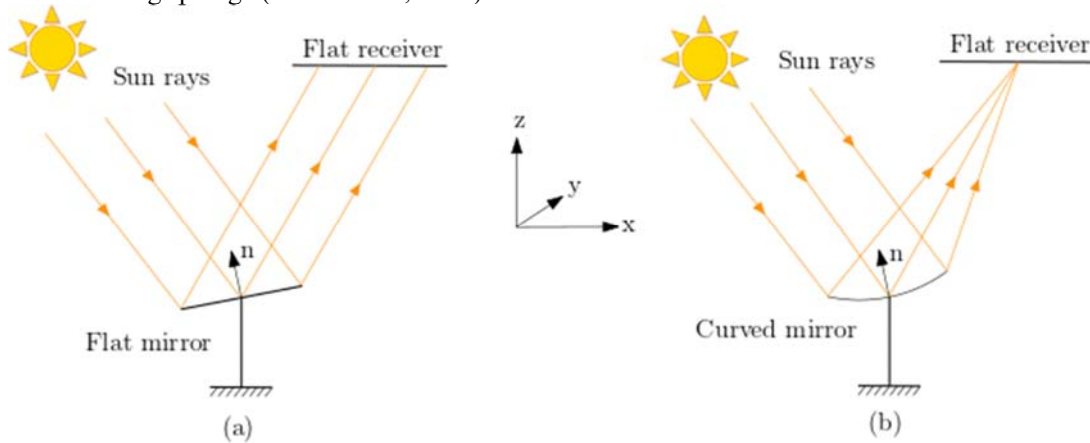

Fig. 13 Reflected rays for a **(a)** flat and **(b)** curved mirror adapted from Benyakhlef *et al.*, (2016)

Although Cheng *et al.* (2018) found that flat, parabolic and cylindrical mirrors can obtain similar optical efficiencies if optimized, the larger reflected radiation profile associated with flat mirrors also requires a larger receiver aperture width. Moreover, flat mirrors limit the concentration ratio that can be achieved within the receiver and therefore the temperature increase that can be obtained within the heat transfer fluid. Cylindrical mirrors, however, are cheaper and can obtain very similar concentration effects when compared to parabolic mirrors (Abbas *et al.*, 2012a; Cheng *et al.*, 2018; Qiu *et al.*, 2016). Pulido-Iparraguirre *et al.* (2019a) investigated different manufacturing processes and the associated geometric quality for flat, parabolic and cylindrically shaped mirrors. It was found that a cylindrical mirror glued by vacuum to a curved plate resulted in the best performance. El Amine and Sallaou (2019) investigated the effect of mirror deformation due to external loading and presented an optimised mirror structure (a trade-off between the structure's weight and optical performance).

In 2008, construction on the 5 MW Kimberlina LFR plant in California, USA was completed (Conlon *et al.*, 2011), allowing the physical testing of the performance of a Once Through Steam Generation plant.

The early mirror fields designed with PV panels in mind have renewed relevance in light of the emergence of Concentrated Photovoltaic (CPV) and Concentrated Photovoltaic/Thermal (CPV/T) hybrid plants. Standard linear Fresnel fields are able to obtain a large degree of uniformity of concentrated solar flux on the PV panel used in place of a thermal receiver within a CPV plant (G. Wang *et al.*, 2020b). Moreover, coupling the cheapest type of CSP field with the significant drop in the price of PV panels presents the prospect of significant cost reductions (Boito and Grena, 2021; Çalık and Fırat, 2019). Using flat mirrors and the condition of no blocking and shading for a vertical sun, Çalık and Fırat, (2019) reported a system efficiency of η_{sys} = 15.8% for a study using solar data from Istanbul, Turkey. G. Wang *et al.* (2020b) reported energy conversion efficiencies of the solar cell monomer and module of 14.7% and 13.6%. These are higher than the equivalent efficiencies obtained using a parabolic trough concentrator (12.3% and 10.7% respectively), but lower than the efficiencies reported for a non-concentration condition (17.9% and 17.1%). These values were validated using an experimental setup in China. Boito and Grena (2021) reported system efficiencies of η_{sys} = 13.99% and η_{sys} = 13.08% for the concentrating and non-concentrating conditions of a plant in the Atacama Desert, while assuming a 5% reduction in efficiency due to nonhomogeneous flux.

While the designs proposed within this section are still used extensively and have obtained new relevance, the other two prominent research avenues focused on design optimisation studies and novel primary mirror field configurations.

5. Design optimisation studies

Early optimisation and sensitivity studies sought to investigate the parameters identified in previous designs as fundamental: the number of mirrors, the gap size between mirrors, mirror width, mirror curvature and receiver height. The objective function used within these studies is typically normalised by the energy available to the mirror field, because using the absorbed radiation as an objective function would simply result in larger mirror aperture areas. In addition to the optical efficiency defined in eq. (3), the exergy efficiency can be used as a measure of the performance of the collector. This efficiency definition represents a measure of 'useful' energy, only incorporating energy with a flux density high enough to provide useful work (Abbas *et al.*, 2012b)

$$\eta_{exergy} = 100 \cdot \frac{\dot{Q}_{inc,rec}(Radiant\ flux\ density \geq 10kW/m^2)}{DNI \cdot A_m} \qquad (26)$$

Given the practical importance of costing to the competitiveness of a technology, some studies are techno-economic in nature, incorporating costing models into the evaluation of the design. Where this is the case, the objective functions used are either the Levelised Cost of Electricity (LCOE/LEC) or the Nominal Cost of Exergy.

Morin *et al.* (2006) reported on the statistical optimisation of a VDemo-Fresnel, an experimental installation with the aim of further preparing for the *FRESDEMO* plant at Plataforma Solar de Almería in Spain. The study independently varied the receiver height, gap between mirrors, number of primary mirrors and mirror curvature and reported on the resultant Levelized Cost of Electricity (LEC). Fig. 13a illustrates the effect of gap size on the levelized cost of electricity. The optimum exists at a trade-off between reducing blocking and shading losses and increasing mirror structure and land costs. While Morin *et al.* (2006) found that variation of the number of primary mirrors resulted in a graph very similar in form to the gap size variation graph (Fig. 13a), Said *et al.* (2019) found that the optical efficiency increased proportionally with the number of primary mirrors used for an experimental system at the University of Blida in Algeria. The transversal and longitudinal optical factors for this same collector can be found in a subsequent paper investigating the use of nanofluids (Said et al., 2021). In contrast, Eddhibi *et al.* (2017) found that using a larger number of mirrors with a constant gap width increased blocking and shading losses, thereby decreasing the optical efficiency of the system.
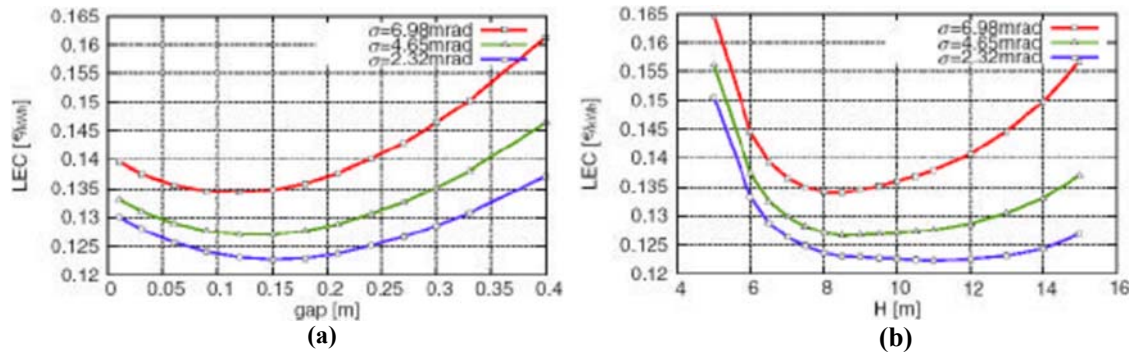
Fig. 14 Effect of the independent variation of **(a)** gap size and **(b)** receiver height on the Levelised Electricity

Cost (LEC) (Morin *et al.*, 2006)

Nixon and Davies (2012) completed a techno-economic study for an experimental prototype in Gujarat, India, using the condition of no blocking and shading for a non-zero transversal onset angle to determine the gap size. Fig. 15 shows that the nominal cost of exergy was relatively constant except for very large gap sizes, while the exergy variation mirrored the changes reflected in the LEC within the study of Morin *et al.* (2006).
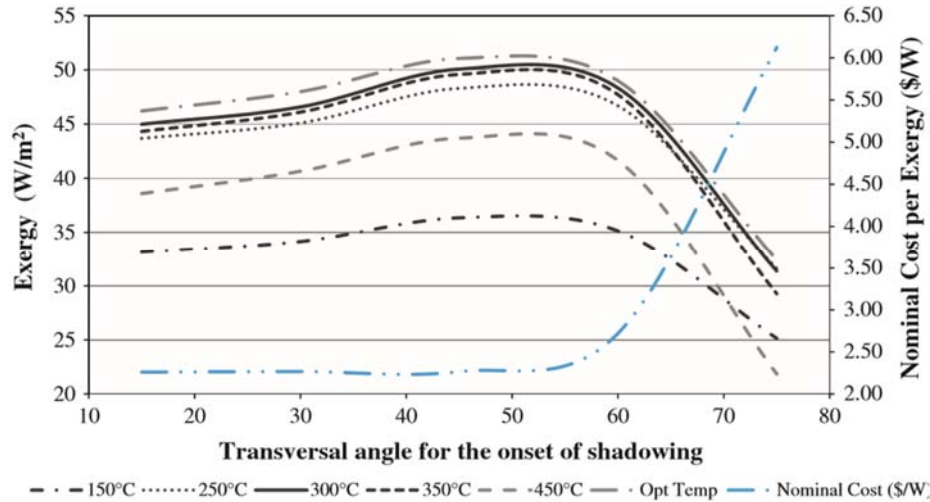
Fig. 15 Exergy and nominal cost per exergy versus the transversal angle specified for the onset of shadowing

(Nixon and Davies, 2012)

Montes *et al.* (2014) investigated the effect of varying receiver height and gap width on the optical, energy and exergy efficiencies, using the *FRESDEMO* plant as a reference. The gap width was expressed in terms of the field width and the filling factor; defined as the ratio between the mirror area and the solar field area for a constant gap width. The maximum annual optical efficiency of η_{opt} = 60% in Fig. 16a was obtained for the largest gap widths (or widest fields) and receiver heights above 10m. While the maximum annual exergy efficiency of η_{exergy} = 47% in Fig. 16b was also obtained for receiver heights above 10m, the optimum field was not the widest field in this case. The use of a higher receiver for the same field width reduces blocking and shading losses, as adjacent mirrors are placed at lower angles (Pulido-Iparraguirre et al., 2019b). The optimum receiver height range obtained by Montes *et al.* (2014) is largely in line with the range reported by Morin *et al.* (2006) except for the case in which the maximum optical error was considered, where the optimum receiver height was closer to 8m. This is likely due to the larger distances associated with higher receivers exacerbating the effects of the optical errors.
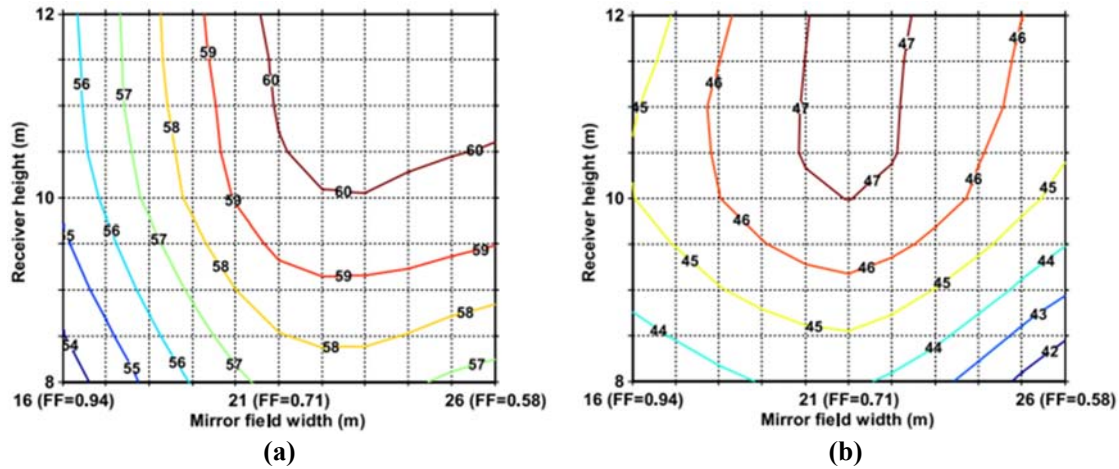
Fig. 16 Annual **(a)** optical and **(b)** exergy efficiency versus receiver height and field width (Montes *et al.*, 2014)

Similarly to Montes *et al.* (2014), Barale *et al.* (2010) reported that the maximum receiver height resulted in the best optical performance for the FERA experimental prototype in Sicily, Italy while González-Mora and Dolores Durán García (2020) reported the same for an LFR field in Sonora, Mexico. In addition to the receiver height, the gap size, mirror curvature, receiver aperture width and depth, as well as receiver tube placement were investigated. The maximum optical performance occurred for a gap size of G = 0.2m (not at the maximum allowable gap size, as found by others) and a mirror curvature of 25m. Moreover, the study demonstrated that allowing the mirror curvature to vary individually further increased the optical performance. This stands to reason, as the mirror curvature corresponds to the focal length of the mirror; allowing for variation in mirror curvature thus allows the focal length calculation to incorporate the mirror position such that all mirrors have the same focal point, as shown in Fig. 13. Boito and Grena (2016) found that allowing the focal lengths to vary nonuniformly had a bigger impact on efficiency than allowing mirror gaps to vary nonuniformly. In contrast, Qiu *et al.* (2017) found that allowing the aiming lines of a field to vary had almost no effect on the optical efficiency. It did however, affect the uniformity of the flux on the receiver.

Given that mirror curvature dictates a mirror's focal length, it is inherently linked to receiver height. A number of studies (Barale *et al.*, 2010; Benyakhlef *et al.*, 2016; Boito and Grena, 2016; Cheng *et al.*, 2018) therefore include both the receiver height and mirror curvature within their optimisation parameters. Benyakhlef *et al.* (2016) investigated the effect of varying mirror curvature and receiver height for the CHAMS-1 in Benguerir, Morocco. They also found that the maximum optical efficiency (η_{opt} = 79%) occurred at the maximum allowable receiver height. However, when using one curvature throughout the entire field, the resultant optical efficiency for a given receiver height was relatively constant except for the extremes of the curvature range. Boito and Grena (2016) optimised the mirror width, gap between mirrors and focal point of the mirrors using the cost per meter of collector divided by the collected radiation (termed the specific cost of the energy collected) as an objective function. The cost function accounted for the costs of the receiver, land area and mirrors by means of a linear function that assumed that the cost was equally distributed across the cost components. They found that allowing the mirror gap and focal length to vary nonuniformly resulted in a 4.46% improvement in the cost of energy relative to the uniformly optimised field. A large variety of parameter combinations achieved relatively similar results in terms of the cost of energy collected, as the objective function was relatively flat. This may in part be due to the fairly general cost function used in the optimisation, potentially affecting the sensitivity of the objective function. Alternative costing models include those built in to annual performance simulation software such as the System Advisory Model used by Ghodbane *et al.* (2021) to assess the performance of an LFR collector in the El-Oued region of Algeria and the model developed through a number of LFR case studies (Filali Baba et al., 2020).

Moghimi *et al.* (2017) generalised the more detailed costing model from Mertins (2009) based on the costs associated with the *Solarmundo* linear Fresnel plant. The number of mirrors, mirror width, gap

and receiver height were all varied within the study, while the focal length of each mirror was calculated such each mirror focussed on the centre of the tube bundle. In addition to the optical parameters, the cavity angle, depth, number of tubes and gap between the tubes were incorporated into the optimization using CFD in combination with a Pareto front that incorporated the optical, thermal and economic objective functions. Cheng *et al.* (2018) and Ajdad *et al.* (2019) both make use of particle swarm optimisation in order to optimise both the primary mirror field and receiver geometry, using the optical efficiency as the objective function. The resultant optimum values for the design parameters are listed in Table 4

Table 4 Optimum parameter values for Moghimi, Cheng and Ajdad optimisations

Parameter	Unit	Symbol	(Moghimi et al., 2017)	(Cheng et al., 2018)			(Ajdad et al., 2019)
Receiver type			Multitube	CPC monotube			CPC monotube
				Flat	Cylindrical	Parabolic	
Receiver height	m	H_R	18.605	11.81	9.49	9.44	4
Mirror focal length	m	f	Dependent	-	12.33	24.75	5.25
Mirror width	mm	w_m	681	250	250	250	410
Gap between mirrors	mm	S_n	23	250	250	250	122
Receiver aperture width	mm	W_A	332	295	295	295	200
Tube position from back of receiver	mm	d_T	105				76.3
Tube outer diameter	mm	OD_T	60.33	200	200	200	70
Gap between parabolic focal points/ tubes	mm	$g_{P/T}$	2	220	220	220	25.6
Optical efficiency	%	η_{opt}		60.29	61.09	61.11	60

Kincaid *et al.* (2019) performed a sensitivity study on the effects of vertical, horizontal and angular displacement for a novel LFR field. The Hyperlight LFR prototype consisted of waterborne mirrors and a monotube receiver with CPC secondary. The maximum geometric intercept factor for the field was $\gamma = 0.8$.

In conclusion, a multitude of design sensitivity and optimisation studies have been conducted over the years using a wide range of techniques. Where early studies simply sought to characterise different variables and derive basic relations between them, subsequent optimisation studies sought to understand the interaction between these variables for a variety of conditions. The drawback to some of these optimisation studies is that they essentially represent a black box, making the drivers of the optimum performance difficult to trace.

6. Novel linear Fresnel primary mirror field configurations

6.1 Compact linear Fresnel

In 1998, Mills and Morrison (2000) proposed interleaving the edges of two standard LFR mirror fields, as indicated in Fig. 17. By alternating targets at the edge of the field, dissimilar target angles were created, which reduced the blocking and shading between adjacent mirrors and allowed the mirrors to be more closely packed, a distinct advantage where space is limited or land costs are particularly high. This configuration is therefore particularly well suited to rooftop installations (Serag-Eldin, 2014).The study also compared a "ganged" configuration (each mirror only targets one receiver throughout the year and therefore a number of mirrors can be mechanically linked) with an "unganged" configuration

(mirrors allowed to change receiver target based on which provides the best optical performance) and only found a 0.2% difference in the optical performance of the two fields. As highlighted in section 4, the first CLFR plant was built in 2003 in New South Wales. Subsequent papers (Pye *et al.*, 2004, 2003) based on this installation primarily focussed on the thermal aspects of the plant rather than the optical aspect.
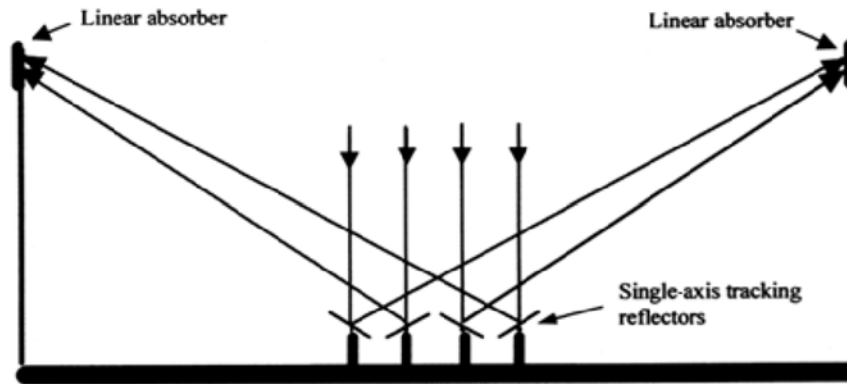

Fig. 17 Compact linear Fresnel field (Mills and Morrison, 2000)

Montes *et al.* (2014) compared the blocking, shading and efficiencies of a standard LFR field, a completely alternating CLFR field (Fig. 18) and hybrid CLFR field (Fig. 19). The mirror width and total field width were kept constant across all the configurations. Increasing the number of mirrors was therefore equivalent to decreasing the gap size between mirrors.
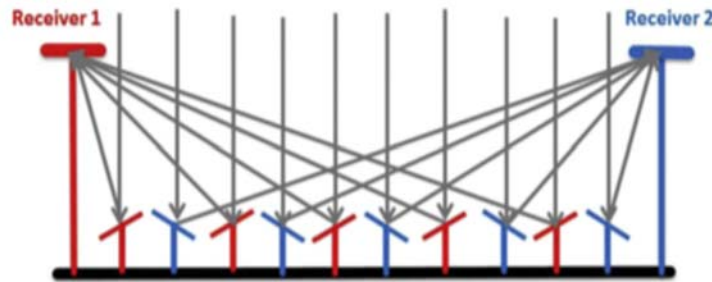

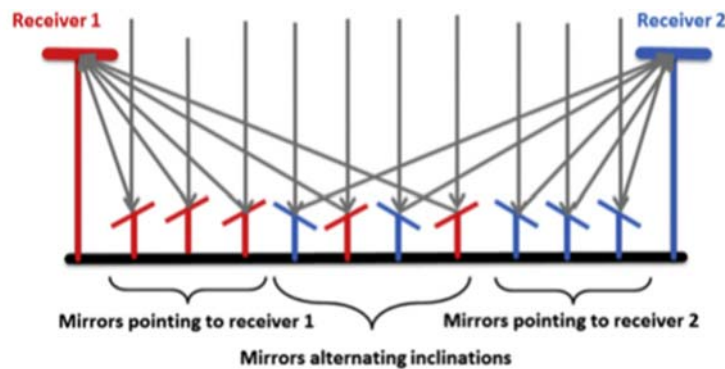**Fig. 18** CLFR field with fully alternating mirrors (Montes *et al.*, 2014)

Fig. 19 CLFR hybrid configuration in which mirrors closest to each receiver exclusively target that receiver while central mirrors alternate (Montes *et al.*, 2014)

Fig. 20 and Fig. 21 (Montes *et al.*, 2014) show that both CLFR configurations have a lower percentage of the total mirror area blocked and shaded than that of the standard LFR configuration. However, as shown in Fig. 22 (Montes *et al.*, 2014), the standard LFR performed marginally better overall. In

addition, the hybrid CLFR system performed better than the fully alternating field, though it is unclear what the optimum point was for the mirrors to start alternating. This was attributed to the additional receiver shading on the field.
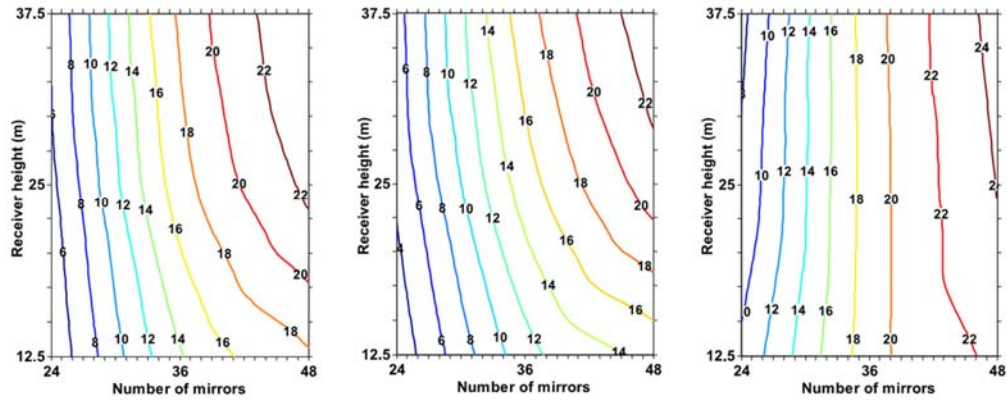

Fig. 20 Percentage area of primary mirrors shaded annually for (a) CLFR hybrid, (b) completely alternating CLFR and (c) LFR fields (Montes *et al*., 2014)
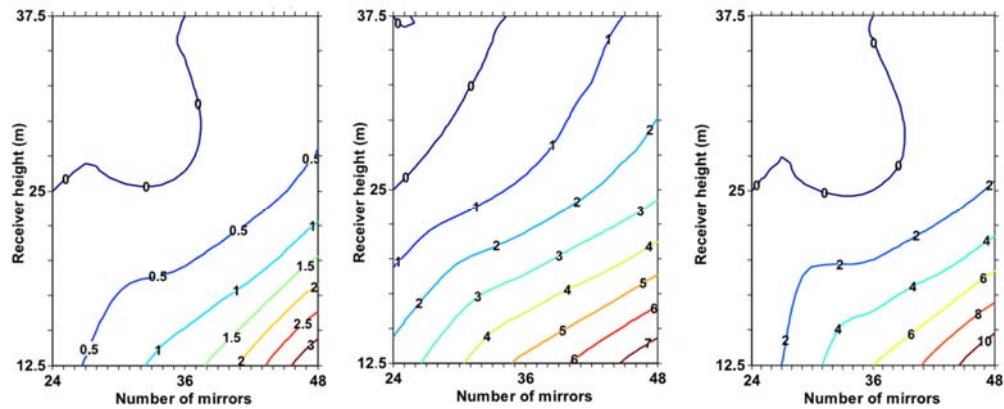

Fig. 21 Percentage area of primary mirrors blocked annually for (a) CLFR hybrid, (b) completely alternating CLFR and (c) LFR fields (Montes *et al*., 2014)
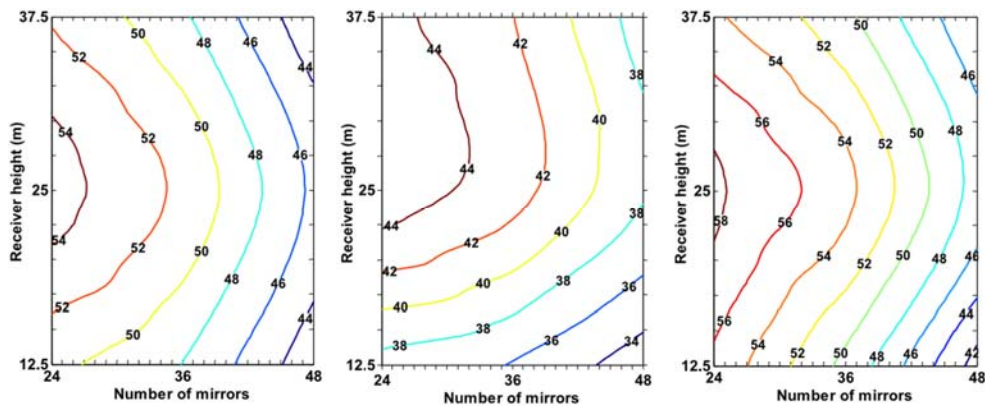

Fig. 22 Annual optical efficiency of a) CLFR hybrid b) completely alternating CLFR and c) LFR fields (Montes *et al*., 2014)

Sharma *et al.* (2016) proposed an adaptation of the LFR analytical model (Sharma et al., 2015a) to quantify the optical losses of a CLFR field. Using a similar methodology, the lost aperture area due to

blocking, shading and end losses could be expressed as a proportion of the total energy of the system. The study allowed the mirrors between the two receivers to target either receiver, based on what was optically most efficient. While the shading loss factor was not significantly affected by the configuration, the cosine loss factor was minimised when mirrors exclusively targeted the receiver closest to them, while the blocking loss factor was minimised for a hybrid configuration. Through varying the mirror spacing and receiver height versus mirror width ratios, minimum Levelized Cost of Electricity values of LCOE = 0.25 \$/kWh and LCOE = 0.24\$/kWh for the ganged and unganged configurations were obtained for Murcia, Spain.

Zhu and Chen (2018) investigated five different primary mirror field configurations. As with Montes *et al*. (2014), the standard central LFR configuration was included to compare the two configurations. The CLFR configurations included were as follows: one completely alternating field and three hybrid fields (A, B, C) in which the percentages of alternating mirrors were 72%, 52% and 36% respectively. The field was designed by adapting the condition of no blocking and shading as shown in Fig. 23 (Zhu and Chen, 2018).
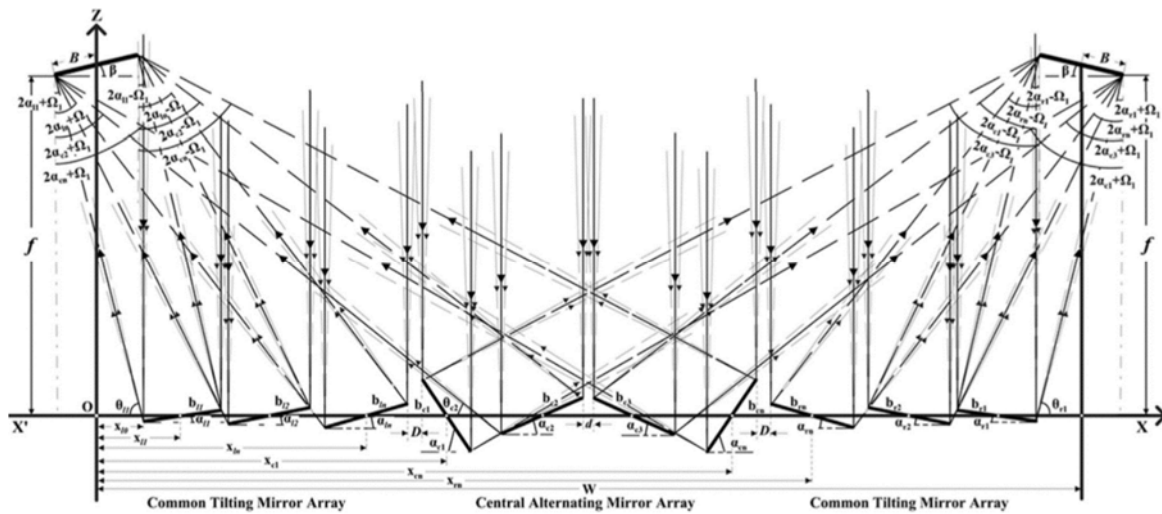

Fig. 23 Compact linear Fresnel field with no blocking and shading for a vertical incoming sun (Zhu and Chen, 2018)

The resultant concentration and utilisation ratios, shown in Fig. 24 (Zhu and Chen, 2018), indicate that hybrid CLFR configurations have higher concentration and utilisation ratios than those of the standard LFR or full CLFR field. In addition, the hybrid configuration that was most densely packed and had the highest percentage of alternating mirrors performed best.
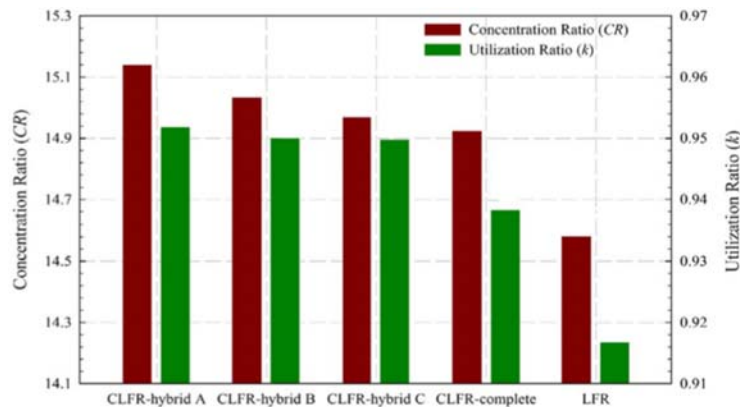

Fig. 24 Concentration and utilisation ratio of CLFR hybrid, CLFR complete and LFR field (Zhu and Chen, 2018)

The simulation results were compared to a small scale experimental CLFR collector constructed in Nottingham, England. The maximum concentration ratio of $C_R = 15.14$ was obtained for a mirror focal length of 1500mm for a horizontal receiver. While the concentration ratio could be further increased by increasing the number of mirrors used in the field, the larger gaps required to maintain the condition of no blocking and shading for a wider field decrease the utilization ratio of the field.

These studies indicate that hybrid compact linear Fresnel fields have the potential to increase the power output and land utilisation of a plant. However, the reduction in blocking and shading losses must be large enough to offset the increase in receiver shading and the losses due to optical errors. Moreover, the optimum transition point from the single-target mirror section to alternating target mirror section must be determined based on the parameters of the field. Babu *et al.* (2020) compared a CLFR field with mirrors of equal width to a field of varying mirror widths, obtaining concentration ratios of $C_R = 103.33$ and $C_R = 85$ respectively.

In addition to the high ground utilisation ratios, CLFR fields have the potential to provide enhanced solar concentration uniformity (Wang *et al.*, 2020), which makes this field a promising candidate for use in the field of Concentrated Photovoltaics (CPV) and hybrid CPV/T. Fig. 25 shows the layout of a hybrid CSP/CPV system with a spectral beam splitter (Wang *et al.*, 2019). In the case of a pure CPV system, only the solar cells would be included in place of the conventional thermal receiver. Wang *et al.* (2020) investigated four CLFR configurations, one with alternating mirrors throughout the field and three hybrid fields with 25%, 55.6% and 88.2% of the mirrors alternating respectively. The field with alternating mirrors throughout the field resulted in the most uniform solar distribution on the panel and also had the highest concentration ratio and filling factor. The simulated solar flux distribution on the panel was validated using an experimental setup in China.
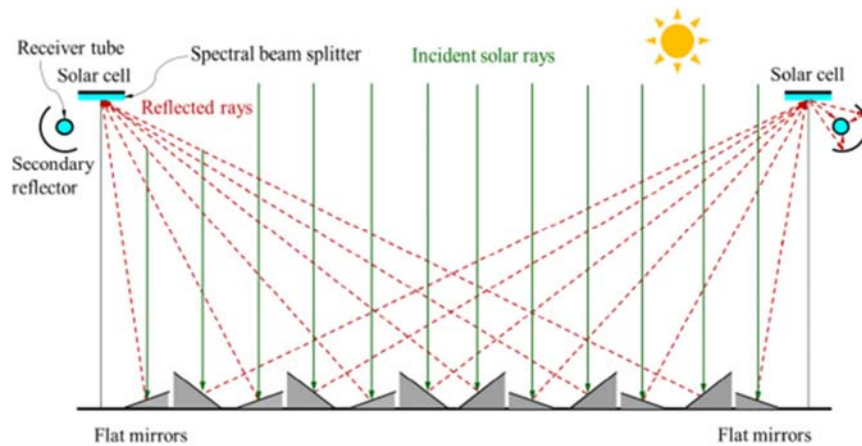

Fig. 25 Hybrid CPV/T system using a CLFR mirror field (Wang *et al.*, 2019)

For a hybrid CPV/T system, the absorber tube height and diameter affected the proportion of energy distributed to the PV and thermal system respectively. While Boito and Grena (2021) questioned whether a hybrid system would increase the efficiency of a CPV system, Wang *et al.* (2019) reported a PV and system efficiency of $\eta_{PV} = 31.2\%$ and $\eta_{sys} = 26.7\%$ for the combined system and a PV and system efficiency of $\eta_{PV} = 25\%$ and $\eta_{sys} = 23.8\%$ for the purely CPV system.

6.2 Translating mirrors and receivers

As end losses play a significant role in the optical efficiency of a small scale LFR field, a number of studies suggest either placing the primary mirror field at a constant tilt angle for a given location (Abbas et al., 2017; Abbas and Martínez-Val, 2017; Barbón et al., 2019; Mills and Morrison, 2000; Pulido-Iparraguirre et al., 2019b), extending the receiver or placing the receiver at an offset (Barbón *et al.*, 2016b; Bellos *et al.*, 2019). Alternatively, a new degree of freedom can be introduced, either in the form of a variable tilt angle (Zhu *et al.*, 2017), mirrors than can translate longitudinally (Yang *et al.*, 2018) or a receiver that can translate longitudinally (Zhu *et al.*, 2016).

Abbas *et al.* (2017) found that tilting the mirror field has a greater effect on the optical efficiency when the collector is oriented along the North-South axis. Moreover, it was determined that each field had an optimum tilt, based on the field parameters and the latitude of the plant. The maximum energy efficiency of η_{en} = 81% for a plant latitude of 37.1° occurred for a field tilt of λ = 33.44°, while for a plant latitude of 24.1° the maximum energy efficiency of η_{en} = 84% occurred for a field tilt of λ = 22.2°. While theoretically the optimum tilt should be very similar to the latitude of the plant, Pulido-Iparraguirre *et al.* (2019) also found that the optimum tilt angle was lower (λ = 25.8° for a plant latitude of 37.1° North), due to seasonal variations in the sun angle. When provision was made for this variation, using an adjustable tilt angle, Zhu *et al.* (2017) reported a 9% increase in the thermal efficiency to η_{th} = 64%. This value was validated using an experimental prototype in Ghangzhou, China. Barbón *et al.* (2019) combined both receiver and mirror tilt for five European locations and found that the maximum energy to area ratios occurred for a receiver tilt equal to the plant latitude, while the mirror tilt was equal to half of the plant latitude. Subsequent studies detail the construction of this small scale LFR (Barbón *et al.*, 2021) and optimise both the individual SSLFR collector and the layout for a given restricted area in which multiple collectors were installed (Bayón-Cueli *et al.*, 2020)

Instead of tilting the collector components, the mirror and/or receiver can be offset in the longitudinal direction. Yang *et al.* (2018) validated the theoretical reduction in end losses for sliding mirrors using an experimental prototype in Nanjing, China. The maximum sliding distance required to reduce end losses completely was proportional to the receiver height and the latitude of the plant, while inversely proportional to the receiver length. For length to receiver height ratios over 5, the annual average optical efficiency remained relatively constant, due to the diminished effect of end losses on the overall efficiency. However, for short LFR collectors the efficiency could be enhanced by up to 50% to an annual average optical efficiency of η_{opt} = 68%. In order to reduce the number of parts moving longitudinally, Bellos *et al.* (2019) proposed extending and/or offsetting the receiver. While increasing the receiver length by 50% resulted in an improvement of the mean IAM of 40.6%, further increase produces diminishing returns. Given that end losses are a function of the longitudinal angle, so too is the optimum receiver displacement; large receiver displacements enhance performance for large longitudinal angles. A relatively small receiver displacement of d_R = 0.2 was found to be the optimum, maximising the IAM to 44.7%. When combining both of these receiver modifications, a yearly mean IAM of 55.3% can be achieved for a length extension of 80% and a displacement of d_R = 0.2. This represents a similar improvement in efficiency (48.7%) to that of Yang *et al.* (2018).

6.3 Semi-parabolic linear Fresnel

Over the years, the optical efficiency of linear Fresnel technology has often been compared unfavourably with that of parabolic trough collectors (Barlev *et al.*, 2011; Cau and Cocco, 2014; El Gharbi *et al.*, 2011; Häberle *et al.*, 2002; Morin *et al.*, 2012; Schenk *et al.*, 2014). Therefore, to increase the optical efficiency of a linear Fresnel collector, a number of studies have proposed elevating individual LFR mirrors to form a curve.

Walker *et al.* (2012; 2013) proposed pivoting mirrors around an offset axis of rotation rather than the mirrors simply rotating around their centres, as shown in Fig. 26a. This modification increased the power production marginally over the course of the day, though it is unclear whether the gain in power production would be sufficient to justify the increased complexity of the system. The resultant field was similar in form the field obtained by placing the axis of the mirrors along a parabolic curve, as shown in Fig. 26b (Zhu and Huang, 2014).
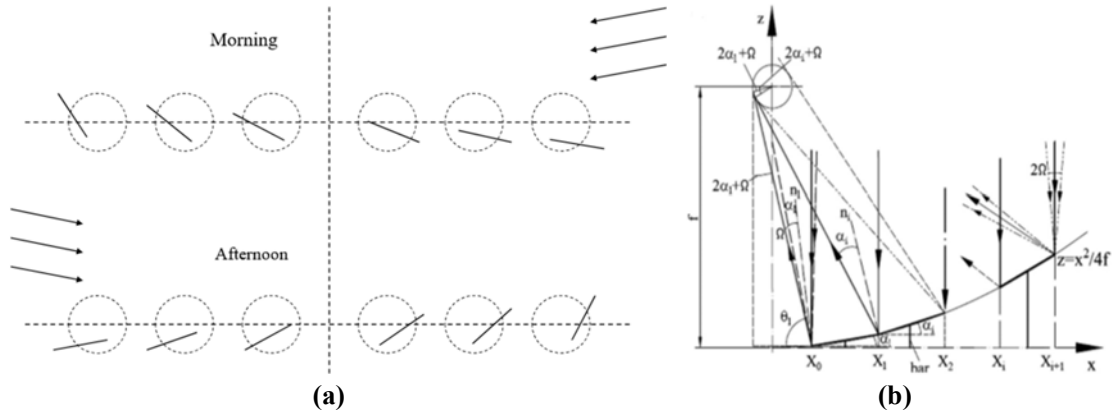
Fig. 26 Primary mirror field layout for **(a)** a field with an offset axis of rotation (Walker *et al.*, 2012) and **(b)** a semi-parabolic LFR field (Zhu and Huang, 2014)

The semi-parabolic field with a tubular receiver obtained the same concentration ratio as the parabolic trough collector tested within the study (C_R = 10.08). The stretched parabolic LFR collector subsequently proposed by Zhu *et al.* (2016) featured an evacuated monotube with CPC secondary that could move longitudinally and mirrors placed along a parabolic curve that could move transversally to expand the gaps between facets. The prototype built in Guangzhou, China obtained a concentration ratio of C_R = 13 (comparable to the concentration ratios obtained by parabolic trough collectors) and an experimental thermal efficiency range of η_{th} = 52 - 66%. The elevated LFR field proposed by Nixon and Davies (2016) also placed mirrors along a parabolic curve and made use of a multitube receiver with CPC secondary. The prototype built in Birmingham, England obtained a maximum thermal efficiency of η_{th} = 70% and a maximum optical efficiency of η_{opt} = 71%. Momeni *et al.* (2019) proposed the use of a several large parabolic mirrors with a tubular receiver. When compared to a flat LFR field, maximum local concentration ratios of LCR_{max} = 44.2 were obtained for the parabolic Fresnel reflector field relative to LCR_{max} = 23.4 for the standard field The resultant LCR distribution was similar in form to that of the semi-parabolic field proposed by Zhu and Huang (2014), as shown in Fig. 27, however it represented a larger increase in the local concentration ratio obtained relative to a standard LFR field. This suggests that even in these semi-parabolic fields, mirror curvature can represent a significant increase in the concentration ratios that can be obtained by the mirror field.
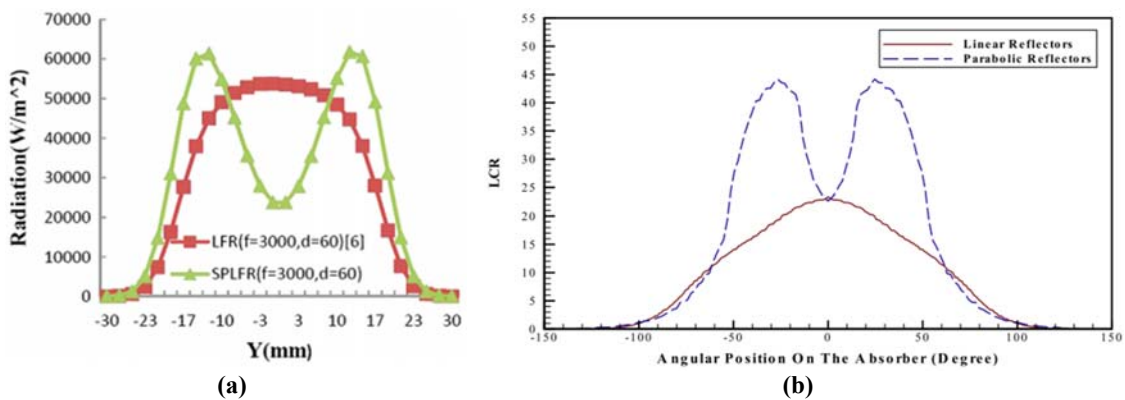

Fig. 27(a) Radiation distribution for flat mirrors placed along a parabolic curve (Zhu and Huang, 2014) **(b)** Local Concentration Ratio for multiple parabolic mirrors (Momeni *et al.*, 2019)

These novel configurations have developed aspects that appear quite similar even though the design process or initial idea used was different. It is likely that the underlying cause of this congruent evolution is that there is a common objective function that governs the form of the optimum design. The most likely objective function is derived from the field of non-imaging optics, namely etendue conservation.

6.4 Etendue-conserving compact linear Fresnel

Etendue is a purely geometric quantity that describes an optical field's flux-gathering capacity (Boyd, 1983). It is defined as the product of the area and the solid angle of the source. As such, it can be thought of as a measure of the "volume" that light occupies in phase space (Chaves, 2016), in the same way that radiance can be thought of as the "energy density" of light. The energy associated with a beam of light is thus the product of its radiance and etendue.

Therefore, etendue conservation can be derived based on the law of conservation of energy (Chaves, 2016). For etendue to be conserved, the etendue of the incoming radiation must be equal to that of the outgoing radiation. Therefore, designing a system where etendue is conserved is analogous to designing a no-loss optical system. Importantly, this single quantity encapsulates all previously discussed optical losses without the computational intensity of individually calculating the energy lost due to each mechanism. A system in which etendue is conserved can be used to establish a theoretical limit for concentration ratios and optical efficiency (Winston *et al.*, 2005).

For a single receiver, a parabolic mirror satisfies the condition of etendue conservation (Canavarro *et al.*, 2013). Therefore, the semi-parabolic LFR fields are closer to a system of etendue conservation than their flat counterparts and consequently, achieve higher optical efficiencies for vertical sun angles. For an etendue-conserving CLFR field with two receivers, the mirrors directly under each receiver will exclusively target that receiver (thus adhering to the parabolic curve) and the mirrors in the central section will split the incoming light into two parts (Chaves and Collares-Pereira, 2010), as shown in Fig. 28.
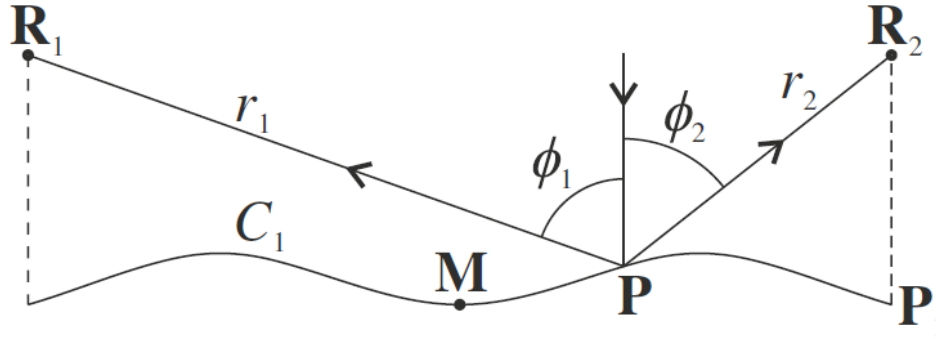

Fig. 28 Etendue-conserving curve for a field with two receivers and a vertical sun (Chaves and Collares-Pereira, 2010)

In order for the etendue of an optical system with two receivers to be conserved, the etendue of the incoming light (dU_0) must be equal to the etendue of the light being reflected onto both receivers (dU_1 and dU_2):

$$dU_0 = dU_1 + dU_2 \qquad (27)$$

This equation can be expressed as a function of the curve angle (ω) and the targeting angle to each receiver (ϕ_1 and ϕ_2):

$$cos\ \omega = cos(\phi_1 - \omega) + cos(\phi_2 + \omega) \qquad (28)$$

The optical intercept (or geometrical efficiency) of this field for a vertical sun was reported as $\gamma = 84$ - 90%, depending on the size of the receiver. Horta *et al.* (2011) conducted ray-tracing simulations on an ECCLFR field with a multitube receiver and Tailored Edge Ray Concentrator secondary and obtained optical efficiencies ranging from $\eta_{opt} = 78.2$ - 69%, depending on the optical errors used in the simulation. Guerreiro *et al.* (2011) compared the annual system efficiency of an ECCLFR plant to that of a parabolic trough plant and standard linear Fresnel plant for two locations (Faro, Portugal and Hurghada, Egypt). The use of an ECCLFR field increased the overall system

efficiency of a standard LFR field by 3.3 - 3.9%, while the parabolic trough further increased the system efficiency by a similar margin. Rungasamy *et al.* (2019) found that once the mirror field was optimised, daily optical efficiencies of $\eta_{opt,daily} = 65\%$, and $\eta_{opt,daily} = 67.9\%$ (geometrical intercepts of $\gamma = 79\%$ and $\gamma = 83\%$) could be obtained for an ideal summer's day for a flat CLFR and ECCLFR respectively. In addition, an offpeak etendue conserving field was proposed, in which mirrors moved up and down throughout the day according to the following curve

$$cos\ (\omega - \theta_T) = cos(\phi_1 - \omega) + cos(\phi_2 + \omega)$$

(29)

This additional degree of freedom resulted in a daily optical efficiency of $\eta_{opt,daily} = 75.4\%$. Table 5 lists several performance metrics for a parabolic trough, standard linear Fresnel, compact linear Fresnel and etendue conserving compact linear Fresnel fields.

Table 5 Performance assessment for a standard parabolic trough, linear Fresnel and etendue conserving compact linear Fresnel field

	Filling factor	Optical efficiency (%)	LCOE (Euro/kWh)
Standard PTC		78 (Guerreiro *et al.*, 2011)	0.305 (Guerreiro *et al.*, 2011)
Standard LFR	0.71 (Canavarro, 2014)	66 (Guerreiro *et al.*, 2011)	0.122 – 0.135 (Morin *et al.*, 2006)
Flat CLFR	0.95 (Zhu and Chen, 2018)		0.2 (Sharma *et al.*, 2016)*
ECCLFR	0.90 (Canavarro, 2014)	74 (Guerreiro *et al.*, 2011)	0.21 (Guerreiro *et al.*, 2011)

* Converted from \$/kWh to €/kWh based on the conversion rate of \$ 1 = € 0.82

While the ECCLFR field has a slightly lower optical efficiency than the standard PTC field, it is significantly higher than the optical efficiency for both LFR and CLFR fields. Moreover, the LCOE for an ECCLFR field is relatively similar to that of the CLFR field, suggesting that the costs are not vastly increased by including the additional structure associated with placing mirrors at different heights.

The resultant performance studies suggest that the use of an etendue-conserving field can significantly enhance the optical performance of a standard linear Fresnel field and a compact linear Fresnel field. Therefore, an etendue-conserving CLFR field represents a promising hybridisation of the benefits of LFR and PTC technology; higher optical efficiencies than for LFR and lower costs and wind loads than for PTC.

7. Conclusion

In conclusion, there are three broad avenues of linear Fresnel primary mirror field design: designing for peak conditions; design optimisation in the conventional LFR layout; and novel linear Fresnel layouts. The condition most frequently stipulated when designing for a vertical sun angle is that the mirrors be placed such that no blocking and shading occur between them. Subsequent studies attempted to optimise for the mirror position and field parameters, predominantly optimising for the optical or exergetic efficiency. Lastly, a number of novel configurations were proposed for linear Fresnel fields. The three major contributions in these configurations were the alternating of targets, the changing of mirror heights and the curving of Fresnel mirrors. While these configurations offer enhanced optical performance, the added complexity of the designs is likely to increase the cost of the primary mirror field. In order to fully assess the potential competitiveness of these configurations, the performance and cost of the field must be compared with those of a standard linear Fresnel field and parabolic trough field.

References

Abbas, R., Martínez-Val, J.M., 2017. A comprehensive optical characterization of linear Fresnel collectors by means of an analytic study. Appl. Energy 185, 1136–1151. https://doi.org/10.1016/j.apenergy.2016.01.065

Abbas, R., Martínez-Val, J.M., 2015. Analytic optical design of linear Fresnel collectors with variable widths and shifts of mirrors. Renew. Energy 75, 81–92. https://doi.org/10.1016/j.renene.2014.09.029

Abbas, R., Montes, M.J., Piera, M., Martínez-Val, J.M., 2012a. Solar radiation concentration features in Linear Fresnel Reflector arrays. Energy Convers. Manag. 54, 133–144. https://doi.org/10.1016/j.enconman.2011.10.010

Abbas, R., Muñoz, J., Martínez-Val, J.M., 2012b. Steady-state thermal analysis of an innovative receiver for linear Fresnel reflectors. Appl. Energy 92, 503–515. https://doi.org/10.1016/j.apenergy.2011.11.070

Abbas, R., Valdés, M., Montes, M.J., Martínez-Val, J.M., 2017. Design of an innovative linear Fresnel collector by means of optical performance optimization: A comparison with parabolic trough collectors for different latitudes. Sol. Energy 153, 459–470. https://doi.org/10.1016/j.solener.2017.05.047

Ajdad, H., Filali Baba, Y., Al Mers, A., Merroun, O., Bouatem, A., Boutammachte, N., 2019. Particle swarm optimization algorithm for optical-geometric optimization of linear fresnel solar concentrators. Renew. Energy 130, 992–1001. https://doi.org/10.1016/j.renene.2018.07.001

Al-Kayiem, H.H., Mohammad, S.T., 2019. Potential of Renewable Energy Resources with an Emphasis on Solar Power in Iraq : An Outlook. MDPI Resour. 8. https://doi.org/10.3390/resources8010042

Babu, M., Sekhar Babu, P., Raj, S.S., Saravanan, S., 2020. Theoretical design, material study and material selection for compact linear Fresnel reflector concentrating system, in: Materials Today: Proceedings. Elsevier Ltd. https://doi.org/10.1016/j.matpr.2020.08.559

Baharoon, D.A., Rahman, H.A., Omar, W.Z.W., Fadhl, S.O., 2015. Historical development of concentrating solar power technologies to generate clean electricity efficiently – A review. Renew. Sustain. Energy Rev. 41, 996–1027. https://doi.org/10.1016/j.rser.2014.09.008

Barale, G., Heimsath, A., Nitz, P., Toro, A., 2010. Optical design of a linear Fresnel collector for Sicily. SolarPaces Conf. 1–7.

Barbón, A., Barbón, N., Bayón, L., Otero, J.A., 2016a. Theoretical elements for the design of a small scale Linear Fresnel Reflector: Frontal and lateral views. Sol. Energy 132, 188–202. https://doi.org/10.1016/j.solener.2016.02.054

Barbón, A., Barbón, N., Bayón, L., Otero, J.A., 2016b. Optimization of the length and position of the absorber tube in small-scale Linear Fresnel Concentrators. Renew. Energy 99, 986–995. https://doi.org/10.1016/j.renene.2016.07.070

Barbón, A., Bayón-Cueli, C., Bayón, L., Ayuso, P.F., 2020. Influence of solar tracking error on the performance of a small-scale linear Fresnel reflector. Renew. Energy 162, 43–54. https://doi.org/10.1016/j.renene.2020.07.132

Barbón, A., Bayón-Cueli, C., Bayón, L., Rodríguez, L., 2019. Investigating the influence of longitudinal tilt angles on the performance of small scale linear Fresnel reflectors for urban applications. Renew. Energy 143, 1581–1593. https://doi.org/10.1016/j.renene.2019.05.106

Barbón, A., Fernández-Rubiera, J.A., Martínez-Valledor, L., Pérez-Fernández, A., Bayón, L., 2021. Design and construction of a solar tracking system for small-scale linear Fresnel reflector with three movements. Appl. Energy 285, 116477. https://doi.org/10.1016/j.apenergy.2021.116477

Barlev, D., Vidu, R., Stroeve, P., 2011. Innovation in concentrated solar power. Sol. Energy Mater. Sol. Cells 95, 2703–2725. https://doi.org/10.1016/j.solmat.2011.05.020

Bayón-Cueli, C., Barbón, A., Bayón, L., Barbón, N., 2020. A cost-energy based methodology for small-scale linear Fresnel reflectors on flat roofs of urban buildings. Renew. Energy 146, 944–959. https://doi.org/10.1016/j.renene.2019.07.005

Bellos, E., 2019. Progress in the design and the applications of linear Fresnel reflectors – A critical review. Therm. Sci. Eng. Prog. 10, 112–137. https://doi.org/10.1016/j.tsep.2019.01.014

Bellos, E., Tzivanidis, C., 2018. Development of analytical expressions for the incident angle modifiers of a linear Fresnel reflector. Sol. Energy 173, 769–779. https://doi.org/10.1016/j.solener.2018.08.019

Bellos, E., Tzivanidis, C., Moghimi, M.A., 2019. Reducing the optical end losses of a linear Fresnel reflector using novel techniques. Sol. Energy 186, 247–256. https://doi.org/10.1016/j.solener.2019.05.020

Beltagy, H., Semmar, D., Lehaut, C., Said, N., 2017. Theoretical and experimental performance analysis of a Fresnel type solar concentrator. Renew. Energy 101, 782–793. https://doi.org/10.1016/j.renene.2016.09.038

Bendt, P., Rabl, A., Gaul, H.W., Reed, K.A., 1979. Optical analysis and optimization of line focus solar collectors.

Benyakhlef, S., Al Mers, A., Merroun, O., Bouatem, A., Boutammachte, N., El Alj, S., Ajdad, H., Erreguragui, Z., Zemmouri, E., 2016. Impact of heliostat curvature on optical performance of linear Fresnel solar concentrators. Renew. Energy 89, 463–474. https://doi.org/10.1016/j.renene.2015.12.018

Bernhard, R., Hein, S., De Lalaing, J., Eck, M., Eickhoff, M., Pfander M, 2008. Linear Fresnel collector demonstration on the PSA part II - commissioning and first performance tests, in: 14th International Symposium on Concentrating Solar Power Chemical Energy Technology.

Blanco, M., Constantinou, M., Corsi, C., Grigoriev, V., Milidonis, K., Panagiotou, C.F., Papanicolas, C.N., Pye, J., 2019. FluxTracer: A Ray Tracer Postprocessor to Assist in the Design and Optimization of Solar Concentrators and Receivers. J. Sol. Energy Eng. Trans. ASME 141, 1–9. https://doi.org/10.1115/1.4042127

Blanco, M., Mutuberria, A., Monreal, A., Albert, R., 2011. Results of the empirical validation of Tonatiuh at Mini-Pegase CNRS-PROMES facility, in: SolarPACES, Seville.

Blanco, M., Santiago, L.R., 2017. Advances in concentrating solar thermal research and technology. Elsevier.

Bode, S.J., Gauché, P., 2012. Review of optical software for use in concentrating solar power systems., in: Proceedings of the Southern African Solar Energy Conference. pp. 1–8.

Boito, P., Grena, R., 2021. Application of a fixed-receiver Linear Fresnel Reflector in concentrating photovoltaics. Sol. Energy 215, 198–205. https://doi.org/10.1016/j.solener.2020.12.024

Boito, P., Grena, R., 2016. Optimization of the geometry of Fresnel linear collectors. Sol. Energy 135, 479–486. https://doi.org/10.1016/j.solener.2016.05.060

Boyd, R.W., 1983. Radiometry and the detection of optical radiation. Wiley.

Buie, D., Monger, A.G., 2004. The effect of circumsolar radiation on a solar concentrating system. Sol. Energy 76, 181–185. https://doi.org/10.1016/j.solener.2003.07.032

Buie, D., Monger, A.G., Dey, C.J., 2003. Sunshape distributions for terrestrial solar simulations. Sol. Energy 74, 113–122. https://doi.org/10.1016/S0038-092X(03)00125-7

Çalık, K., Fırat, C., 2019. A Cost-Effective Theoretical Novel Configuration of Concentrated Photovoltaic System with Linear Fresnel Reflectors. J. Polytech. 0900, 583–589. https://doi.org/10.2339/politeknik.523704

Canavarro, D., 2014. Advances in the design of solar concentrators for thermal applications. Ph.D. Thesis, University of Evora, Portugal.

Canavarro, D., Chaves, J., Collares-Pereira, M., 2013. Infinitesimal etendue and Simultaneous Multiple Surface (SMS) concentrators for fixed receiver troughs. Sol. Energy 97, 493–504. https://doi.org/10.1016/j.solener.2013.09.012

Cardona, G., Pujol-Nadal, R., 2020. OTSun, a python package for the optical analysis of solar-thermal collectors and photovoltaic cells with arbitrary geometry. PLoS One 15, 1–15. https://doi.org/10.1371/journal.pone.0240735

Cardoso, J.P., Mutuberria, A., Marakkos, C., Schoettl, P., Osório, T., Les, I., 2018. New functionalities for the Tonatiuh ray-tracing software. AIP Conf. Proc. 2033. https://doi.org/10.1063/1.5067212

Cau, G., Cocco, D., 2014. Comparison of medium-size concentrating solar power plants based on parabolic trough and linear Fresnel collectors, in: Energy Procedia. Elsevier Ltd, pp. 101–110. https://doi.org/10.1016/j.egypro.2014.01.012

Chai, J.C., Lee, H.O.S., Patankar, S. V., 1993. Ray effect and false scattering in the discrete ordinates method. Numer. Heat Transf. Part B Fundam. 24, 373–389. https://doi.org/10.1080/10407799308955899

Chaves, J., 2016. Introduction to nonimaging optics. Taylor & Francis.

Chaves, J., Collares-Pereira, M., 2010. Etendue-matched two-stage concentrators with multiple receivers. Sol. Energy 84, 196–207. https://doi.org/10.1016/j.solener.2009.10.022

Cheng, Z.D., Zhao, X.R., He, Y.L., Qiu, Y., 2018. A novel optical optimization model for linear Fresnel reflector concentrators. Renew. Energy 129, 486–499. https://doi.org/10.1016/j.renene.2018.06.019

Coelho, P.J., 2014. Advances in the discrete ordinates and finite volume methods for the solution of radiative heat transfer problems in participating media. J. Quant. Spectrosc. Radiat. Transf. 145, 121–146. https://doi.org/10.1016/j.jqsrt.2014.04.021

Coelho, P.J., 2002. The role of ray effects and false scattering on the accuracy of the standard and modified discrete ordinates methods. J. Quant. Spectrosc. Radiat. Transf. 73, 231–238.

Conlon, W.M., Johnson, P., Hanson, R., 2011. Superheated steam from CLFR solar steam generators, in: Proceedings of the ASME 2011 Power Conference. pp. 1–7.

Craig, K.J., Moghimi, M.A., Rungasamy, A.E., Marsberg, J., Meyer, J.P., 2016. Finite-volume ray tracing using computational fluid dynamics in linear focus CSP applications. Appl. Energy 183, 241–256. https://doi.org/10.1016/j.apenergy.2016.08.154

Desai, N.B., Bandyopadhyay, S., 2015. Integration of parabolic trough and linear Fresnel collectors for optimum design of concentrating solar thermal power plant. Clean Technol. Environ. Policy 17, 1945–1961. https://doi.org/10.1007/s10098-015-0918-9

Eck, M., Hirsch, T., Feldhoff, J.F., Kretschmann, D., Dersch, J., Gavilan Morales, A., Gonzalez-Martinez, L., Bachelier, C., Platzer, W., Riffelmann, K.J., Wagner, M., 2014. Guidelines for CSP yield analysis - Optical losses of line focusing systems; definitions, sensitivity analysis and modeling approaches, in: Energy Procedia. Elsevier Ltd, pp. 1318–1327. https://doi.org/10.1016/j.egypro.2014.03.141

Eddhibi, F., Amara, M. Ben, Balghouthi, M., Qoaider, L., Guizani, A.A., 2017. Analytic optical design of a Linear Fresnel solar collector with variable parameters. J. Mater. Environ. Sci. 8, 4068–4084.

El Amine, M., Sallaou, M., 2019. Integration of mechanical deformation and optical losses in the design of linear Fresnel solar collectors. Int. J. Interact. Des. Manuf. 13, 831–840. https://doi.org/10.1007/s12008-019-00542-1

El Gharbi, N., Derbal, H., Bouaichaoui, S., Said, N., 2011. A comparative study between parabolic trough collector and linear Fresnel reflector technologies, in: Energy Procedia. pp. 565–572. https://doi.org/10.1016/j.egypro.2011.05.065

Evans, D.L., 1977. On the performance of cylindrical parabolic solar concentrators with flat absorbers. Sol. Energy 19, 379–385. https://doi.org/10.1016/0038-092X(77)90009-3

Fan, M., You, S., Xia, J., Zheng, W., Zhang, H., Liang, H., Li, X., Li, B., 2018. An optimized Monte Carlo ray tracing optical simulation model and its applications to line-focus concentrating solar collectors. Appl. Energy 225, 769–781. https://doi.org/10.1016/j.apenergy.2018.05.067

Feuermann, D., Gordon, J.M., 1991. Analysis of a two-stage linear fresnel reflector solar concentrator. J. Sol. Energy Eng. 113, 272–279. https://doi.org/10.1115/1.2929973

Filali Baba, Y., Ajdad, H., Al Mers, A., Bouatem, A., Bououlid Idrissi, B., El Alj, S., 2020. Preliminary cost-effectiveness assessment of a Linear Fresnel Concentrator: Case studies. Case Stud. Therm. Eng. 22, 100730. https://doi.org/10.1016/j.csite.2020.100730

Fossa, M., Boccalatte, A., Memme, S., 2021. Solar Fresnel modelling, geometry enhancement and 3D ray tracing analysis devoted to different energy efficiency definitions and applied to a real facility. Sol. Energy 216, 75–89. https://doi.org/10.1016/j.solener.2020.12.047

Ghodbane, M., Bellos, E., Said, Z., Boumeddane, B., Khechekhouche, A., Sheikholeslami, M., Ali, Z.M., 2021. Energy, Financial, and Environmental Investigation of a Direct Steam Production Power Plant Driven by Linear Fresnel Solar Reflectors. J. Sol. Energy Eng. 143. https://doi.org/10.1115/1.4048158

Giostri, A., Binotti, M., Silva, P., Macchi, E., Manzolini, G., 2011. Comparison of two linear collectors in solar thermal plants: Parabolic trough Vs Fresnel, in: Proceedings of the ASME 2011 5th International Conference on Energy Sustainability. ASME, Washington, DC, USA.

González-Mora, E., Dolores Durán García, M., 2020. Methodology for an opto-geometric optimization of a linear Fresnel reflector for direct steam generation. Energies 13. https://doi.org/10.3390/en13020355

Goodwin, P., Williams, R.G., Ridgwell, A., 2015. Sensitivity of climate to cumulative carbon emissions due to compensation of ocean heat and carbon uptake. Nat. Geosci. 8, 29–34. https://doi.org/10.1038/ngeo2304

Goswami, R.P., Negi, B., Sehgal, H.K., Sootha, G.D., 1990. Optical designs and concentration characteristics of a linear Fresnel reflector solar concentrator with a triangular absorber. Sol. Energy Mater. 21, 237–251. https://doi.org/10.1016/0741-983X(90)90023-U

Guerreiro, L., Canavarro, D., Collares-Pereira, M., 2011. Increasing the cost effectiveness of CSP technologies through the development of a new CLFR "etendue matched" collector, in: 30th ISES Biennial Solar World Congress 2011, SWC 2011. pp. 3878–3886. https://doi.org/10.18086/swc.2011.25.14

Häberle, A., Zahler, C., Lalaing, J. De, Ven, J., Sureda, M., Graf, W., Lerchenmüller, H., Wittwer, V., 2000. The Solarmundo Project - Advanced Technology for Solar Thermal Power Generation.

Häberle, A., Zahler, C., Lerchenmüller, H., Mertins, M., Wittwer, C., Trieb, F., Dersch, J., 2002. The Solarmundo line focussing Fresnel collector. Optical and thermal performance and cost calculations.

He, Y.L., Wang, K., Qiu, Y., Du, B.C., Liang, Q., Du, S., 2019. Review of the solar flux distribution in concentrated solar power: Non-uniform features, challenges, and solutions. Appl. Therm. Eng. 149, 448–474. https://doi.org/10.1016/j.applthermaleng.2018.12.006

Heimsath, A., Bern, G., Van Rooyen, D., Nitz, P., 2014. Quantifying optical loss factors of small linear concentrating collectors for process heat application, in: Energy Procedia. Elsevier Ltd, pp. 77–86. https://doi.org/10.1016/j.egypro.2014.02.010

Hertel, J.D., Martinez-Moll, V., Pujol-Nadal, R., 2016. Influence of thermal losses on the incidence angle modifier factorization approach. Sol. Energy 135, 50–58. https://doi.org/10.1016/j.solener.2016.05.035

Hertel, J.D., Martinez-Moll, V., Pujol-Nadal, R., 2015. Estimation of the influence of different incidence angle modifier models on the biaxial factorization approach. Energy Convers. Manag. 106, 249–259. https://doi.org/10.1016/j.enconman.2015.08.082

Hofer, A., Büchner, D., Kramer, K., Fahr, S., Heimsath, A., Platzer, W.J., Scholl, S., 2015. Comparison of two different (quasi-) dynamic testing methods for the performance evaluation of a linear Fresnel process heat collector, in: Energy Procedia. Elsevier Ltd, pp. 84–95. https://doi.org/10.1016/j.egypro.2015.03.011

Hongn, M., Larsen, S.F., Gea, M., Altamirano, M., 2015. Least square based method for the estimation of the optical end loss of linear Fresnel concentrators. Sol. Energy 111, 264–276. https://doi.org/10.1016/j.solener.2014.10.042

Horta, P., Collares-pereira, M., Canavarro, D., Guerreiro, L.L., 2011. Modeling thermal losses in a new CLFR etendue matched non-evacuated collector cavity, in: SolarPACES 2011, Grenada, Spain. pp. 1–6.

Horta, P., Osório, T., 2013. Optical characterization parameters for line-focusing solar concentrators: Measurement procedures and extended simulation results, in: Energy Procedia. Elsevier B.V., pp. 98–108. https://doi.org/10.1016/j.egypro.2014.03.011

Huang, F., Li, L., Huang, W., 2014. Optical performance of an azimuth tracking linear Fresnel solar concentrator. Sol. Energy 108, 1–12. https://doi.org/10.1016/j.solener.2014.06.028

Hunter, B., Guo, Z., 2015. Numerical smearing, ray effect, and angular false scattering in radiation transfer computation. Int. J. Heat Mass Transf. 81, 63–74. https://doi.org/10.1016/j.ijheatmasstransfer.2014.10.014

International Energy Agency, 2020a. Global Energy Review 2020, Global Energy Review 2020. https://doi.org/10.1787/a60abbf2-en

International Energy Agency, 2020b. World Energy Outlook 2020 [WWW Document]. URL https://www.iea.org/reports/world-energy-outlook-2020 (accessed 5.1.21).

International Renewable Energy Agency, 2020. How Falling Costs Make Renewables a Cost-effective Investment [WWW Document]. URL /newsroom/articles/2020/Jun/How-Falling-Costs-Make-Renewables-a-Cost-effective-Investment

Kalogirou, S.A., 2014. Solar Energy Engineering: Processes and Systems, 2nd ed. ed, Solar Energy Engineering. Elsevier. https://doi.org/10.1016/b978-0-12-397270-5.00010-8

Kincaid, N., Mungas, G., Kramer, N., Wagner, M., Zhu, G., 2018. An optical performance comparison of three concentrating solar power collector designs in linear Fresnel, parabolic trough, and central receiver. Appl. Energy 231, 1109–1121. https://doi.org/10.1016/j.apenergy.2018.09.153

Kincaid, N., Mungas, G., Kramer, N., Zhu, G., 2019. Sensitivity analysis on optical performance of a novel linear Fresnel concentrating solar power collector. Sol. Energy 180, 383–390. https://doi.org/10.1016/j.solener.2019.01.054

Li, H.-S., 2004. Reduction of false scattering in arbitrarily specified discrete directions of the discrete ordinates method. J. Quant. Spectrosc. Radiat. Transf. 86, 215–222. https://doi.org/10.1016/j.jqsrt.2003.08.005

Li, L., Sun, J., Li, Y., He, Y.L., Xu, H., 2019. Transient characteristics of a parabolic trough direct-steam-generation process. Renew. Energy 135, 800–810. https://doi.org/10.1016/j.renene.2018.12.058

Liu, H., Zhou, H., Wang, D., Han, Y., 2020. Performance comparison of two monte carlo ray-tracing methods for calculating radiative heat transfer. J. Quant. Spectrosc. Radiat. Transf. 256, 107305. https://doi.org/10.1016/j.jqsrt.2020.107305

López-Núñez, O.A., Alfaro-Ayala, J.A., Jaramillo, O.A., Ramírez-Minguela, J.J., Castro, J.C., Damian-Ascencio, C.E., Cano-Andrade, S., 2020a. A numerical analysis of the energy and entropy generation rate in a Linear Fresnel Reflector using computational fluid dynamics. Renew. Energy 146, 1083–1100. https://doi.org/10.1016/j.renene.2019.06.144

López-Núñez, O.A., Alfaro-Ayala, J.A., Ramírez-Minguela, J.J., Belman-Flores, J.M., Jaramillo, O.A., 2020b. Optimization of a Linear Fresnel Reflector Applying Computational Fluid Dynamics, Entropy Generation Rate and Evolutionary Programming. Renew. Energy 152, 698–712. https://doi.org/10.1016/j.renene.2020.01.105

Lovegrove, K., Stein, W., 2020. Concentrating Solar Power Technology Principles, Developments, and Applications, 2nd ed. ed. Woodhead Publishing.

Mahan, J.R., 2019. The Monte Carlo ray-trace method in radiation heat transfer and applied optics. Wiley, New Jersey.

Mathur, S.S., Kandpal, T.C., Negi, B.S., 1991. Optical design and concentration characteristics of linear Fresnel reflector solar concentrators - I. Mirror elements of varying width. Energy Convers. Manag. 31, 205–219.

Mathur, S. S., Kandpal, T.C., Negi, B.S., 1991. Optical design and concentration characteristics of linear Fresnel reflector solar concentrators- II. Mirror elements of equal width. Energy Convers. Manag. 31, 221–232.

McIntire, W.R., 1982. Factored approximations for biaxial incident angle modifiers. Sol. Energy 29, 315–322. https://doi.org/10.1016/0038-092X(82)90246-8

Mertins, M., 2009. Technische und wirtschaftliche analyse von horizontalen Fresnel-kollektoren. Ph.D. Thesis, Universität Karlsruhe, Germany.

Miller, W.F., Reed, W.H., 1977. Ray-effect mitigation methods for two-dimensional neutron transport theory. Nucl. Sci. Eng. 62, 391–411. https://doi.org/10.13182/NSE62-391

Mills, D.R., Morrison, G.L., 2000. Compact linear Fresnel reflector solar thermal powerplants. Sol. Energy 68, 263–283. https://doi.org/10.1016/S0038-092X(99)00068-7

Modest, M.F., 2013. Chapter 8 - The Monte Carlo Method for Surface Exchange, in: Modest, M.F. (Ed.), Radiative Heat Transfer (Third Edition). Academic Press, Boston, pp. 247–266. https://doi.org/https://doi.org/10.1016/B978-0-12-386944-9.50008-X

Moghimi, M.A., 2017. Optical, thermal and economic optimisation of a linear Fresnel collector. Ph.D. Thesis University of Pretoria, South Africa.

Moghimi, M.A., Craig, K.J., Meyer, J.P., 2015. A novel computational approach to combine the optical and thermal modelling of linear Fresnel collectors using the finite volume method. Sol. Energy 116, 407–427. https://doi.org/10.1016/j.solener.2015.04.014

Moghimi, M.A., Craig, K.J.J., Meyer, J.P.P., 2017. Simulation-based optimisation of a linear Fresnel collector mirror field and receiver for optical, thermal and economic performance, Solar Energy. Elsevier Ltd. https://doi.org/10.1016/j.solener.2017.06.001

Moghimi, M.A., Rungasamy, A., Craig, K.J., Meyer, J.P., 2016. Introducing CFD in the optical simulation of linear Fresnel collectors, in: AIP Conference Proceedings. https://doi.org/10.1063/1.4949039

Momeni, S., Menbari, A., Alemrajabi, A.A., Mohammadi, P., 2019. Theoretical performance analysis of new class of Fresnel concentrated solar thermal collector based on parabolic reflectors. Sustain. Energy Technol. Assessments 31, 25–33. https://doi.org/10.1016/j.seta.2018.11.004

Montenon, A.C., Tsekouras, P., Tzivanidis, C., Bibron, M., Papanicolas, C., 2019. Thermo-optical modelling of the linear Fresnel collector at the Cyprus institute, in: AIP Conference Proceedings. https://doi.org/10.1063/1.5117613

Montes, M.J., Rubbia, C., Abbas, R., Martínez-Val, J.M., 2014. A comparative analysis of configurations of linear fresnel collectors for concentrating solar power. Energy 73, 192–203. https://doi.org/10.1016/j.energy.2014.06.010

Morin, G., Dersch, J., Platzer, W., Eck, M., Häberle, A., 2012. Comparison of linear Fresnel and parabolic trough collector power plants. Sol. Energy 86, 1–12. https://doi.org/10.1016/j.solener.2011.06.020

Morin, G., Platzer, W., Eck, M., Uhlig, R., Berger, M., Zarza, E., Häberle, A., Berger, M., Zarza, E., 2006. Road map towards the demonstration of a linear Fresnel collector using a single tube receiver. Proc. 13th SolarPACES Int. Symp. 20-23 June 2006 1–11.

Negi, B., Kandpal, T., Mathur, S., 1990. Design and performance characteristics of a linear Fresnel reflector solar concentrator with a flat vertical absorber. Sol. Wind Technol. 7, 379–392.

Negi, B., Mathur, S., Kandpal, T., 1989. Optical and thermal performance of a linear Fresnel reflector solar concentrator. Sol. Wind Technol. 6, 589–593.

Negi, B.S., Bhowmik, N.C., Mathur, S.S., Kandpal, T.C., 1985. Solar limb darkening and ray trace evaluation of solar concentrators. Appl. Opt. 24, 296. https://doi.org/10.1364/ao.24.000296

Neumann, A., Witzke, A., Jones, S.A., Schmitt, G., 2002. Representative terrestrial solar brightness profiles. J. Sol. Energy Eng. Trans. ASME 124, 198–204. https://doi.org/10.1115/1.1464880

Nixon, J.D., Davies, P.A., 2016. Construction and Experimental Study of an Elevation Linear Fresnel Reflector. J. Sol. Energy Eng. Trans. ASME 138, 1–10. https://doi.org/10.1115/1.4032682

Nixon, J.D., Davies, P.A., 2012. Cost-exergy optimisation of linear Fresnel reflectors. Sol. Energy 86, 147–156. https://doi.org/10.1016/j.solener.2011.09.024

Osório, T., Horta, P., Larcher, M., Pujol-Nadal, R., Hertel, J., Van Rooyen, D.W., Heimsath, A., Schneider, S., Benitez, D., Frein, A., Denarie, A., 2016. Ray-tracing software comparison for linear focusing solar collectors, in: AIP Conference Proceedings. https://doi.org/10.1063/1.4949041

Pino, F.J., Caro, R., Rosa, F., Guerra, J., 2013. Experimental validation of an optical and thermal model of a linear Fresnel collector system. Appl. Therm. Eng. 50, 1463–1471. https://doi.org/10.1016/j.applthermaleng.2011.12.020

Pulido-Iparraguirre, D., Valenzuela, L., Fernández-Reche, J., Galindo, J., Rodríguez, J., Zhu, G., Lewandowski, A., 2019., ،.م, شكري‎a. Design, Manufacturing and Characterization of Linear Fresnel Reflector's Facets. Energies 12, 1–15. https://doi.org/10.1115/1.4024247

Pulido-Iparraguirre, D., Valenzuela, L., Serrano-Aguilera, J.J., Fernández-García, A., 2019b. Optimized design of a linear Fresnel reflector for solar process heat applications. Renew. Energy 131, 1089–1106. https://doi.org/10.1016/j.renene.2018.08.018

Pulido, D., Serrano, J.J., Valenzuela, L., Fernández-García, A., 2017. Optimizing Design of a Linear Fresnel Reflector for Process Heat Supply 1–9. https://doi.org/10.18086/eurosun.2016.02.21

Pye, J.D., Morrison, G.L., Behnia, M., 2003. Transient Modelling of cavity receiver heat transfer for the compact linear Fresnel reflector. Manuf. Eng. 1–9.

Pye, J.D., Morrison, G.L., Mills, D.R., Le Lièvre, P., Behnia, M., 2004. Steam-circuit Model for the Compact Linear Fresnel Reflector Prototype. Sol. 2004 1–10.

Qiu, Y., He, Y.L., Cheng, Z.D., Wang, K., 2015. Study on optical and thermal performance of a linear Fresnel solar reflector using molten salt as HTF with MCRT and FVM methods. Appl. Energy 146, 162–173. https://doi.org/10.1016/j.apenergy.2015.01.135

Qiu, Y., He, Y.L., Wu, M., Zheng, Z.J., 2016. A comprehensive model for optical and thermal characterization of a linear Fresnel solar reflector with a trapezoidal cavity receiver. Renew. Energy 97, 129–144. https://doi.org/10.1016/j.renene.2016.05.065

Qiu, Y., Li, M.J., Wang, K., Liu, Z. Bin, Xue, X.D., 2017. Aiming strategy optimization for uniform flux distribution in the receiver of a linear Fresnel solar reflector using a multi-objective genetic algorithm. Appl. Energy 205, 1394–1407. https://doi.org/10.1016/j.apenergy.2017.09.092

Rabl, A., Bendt, P., 1982. Effect of circumsolar radiation on performance of focusing collectors. J. Sol. Energy Eng. Trans. ASME 104, 237–250. https://doi.org/10.1115/1.3266308

Raithby, G.D., 1999. Evaluation of discretization errors in finite-volume radiant heat transfer predictions. Numer. Heat Transf. Part B Fundam. 36, 241–264. https://doi.org/10.1080/104077999275631

Ries, H., Rabl, A., 1994. Edge-ray principle of nonimaging optics. J. Opt. Soc. Am. A 11, 2627. https://doi.org/10.1364/josaa.11.002627

Rönnelid, M., Perers, B., Karlsson, B., 1997. On the factorisation of incidence angle modifiers for CPC collectors. Sol. Energy 59, 281–286. https://doi.org/10.1016/S0038-092X(97)00016-9

Rungasamy, A.E., 2020. Performance assessment and optimisation of different configurations of etendue-conserving compact linear Fresnel solar fields. Ph.D. Thesis, University of Pretoria, South Africa.

Rungasamy, A.E., Craig, K.J., Meyer, J.P., 2019. Comparative study of the optical and economic performance of etendue-conserving compact linear Fresnel reflector concepts. Sol. Energy 181. https://doi.org/10.1016/j.solener.2019.01.081

Said, Z., Ghodbane, M., Hachicha, A.A., Boumeddane, B., 2019. Optical performance assessment of a small experimental prototype of linear Fresnel reflector. Case Stud. Therm. Eng. 16, 100541. https://doi.org/10.1016/j.csite.2019.100541

Said, Z., Ghodbane, M., Sundar, L.S., Tiwari, A.K., Sheikholeslami, M., Boumeddane, B., 2021. Heat transfer, entropy generation, economic and environmental analyses of linear fresnel reflector using novel rGO-Co3O4 hybrid nanofluids. Renew. Energy 165, 420–437. https://doi.org/10.1016/j.renene.2020.11.054

Sait, H.H., Martinez-Val, J.M., Abbas, R., Munoz-Anton, J., 2015. Fresnel-based modular solar fields for performance/cost optimization in solar thermal power plants: A comparison with parabolic trough collectors. Appl. Energy 141, 175–189. https://doi.org/10.1016/j.apenergy.2014.11.074

Schenk, H., Hirsch, T., Feldhoff, J.F., Wittmann, M., 2014. Energetic comparison of linear Fresnel and parabolic trough collector systems. J. Sol. Energy Eng. Trans. ASME 136, 1–11. https://doi.org/10.1115/1.4027766

Schubnell, M., 1992. Sunshape and its influence on the flux distribution in imaging solar concentrators. J. Sol. Energy Eng. Trans. ASME 114, 260–266. https://doi.org/10.1115/1.2930015

Serag-Eldin, M.A., 2014. Thermal design of a roof-mounted CLFR collection system for a desert absorption chiller. Int. J. Sustain. Energy 33, 506–524. https://doi.org/10.1080/14786451.2012.761998

Sharma, V., Khanna, S., Nayak, J.K., Kedare, S.B., 2016. Effects of shading and blocking in compact linear Fresnel reflector field. Energy 94, 114–138. https://doi.org/10.1016/j.energy.2015.10.098

Sharma, V., Nayak, J.K., Kedare, S.B., 2015a. Effects of shading and blocking in linear Fresnel reflector field. Sol. Energy 113, 114–138. https://doi.org/10.1016/j.energy.2015.10.098

Sharma, V., Nayak, J.K., Kedare, S.B., 2015b. Comparison of line focusing solar concentrator fields considering shading and blocking. Sol. Energy 122, 924–939. https://doi.org/10.1016/j.solener.2015.10.011

Singh, R.N., Mathur, S.S., Kandpal, T.C., 1980. Some geometrical design aspects of a linear Fresnel. Energy Res. 4, 59–67.

Singhal, A.K., Sharma, M.S., Negi, B.S., Mathur, S.S., 1986. Performance testing of a linear Fresnel reflector. Int. J. Energy Res. 10, 39–46. https://doi.org/10.1002/er.4440100105

Singhal, A.K., Singh, R.N., Kandpal, T.C., Mathur, S.S., 1982. Geometrical concentration characteristics of a linear Fresnel reflector using a fin receiver. Opt. Appl. XII.

Sootha, G.D., Negi, B.S., 1994. A comparative study of optical designs and solar flux concentrating characteristics of a linear fresnel reflector solar concentrator with tubular absorber. Sol. Energy Mater. Sol. Cells 32, 169–186. https://doi.org/10.1016/0927-0248(94)90302-6

Sun, J., Zhang, Zhi, Wang, L., Zhang, Zhenwen, Wei, J., 2020. Comprehensive Review of Line-Focus Concentrating Solar Thermal Technologies: Parabolic Trough Collector (PTC) vs Linear Fresnel Reflector (LFR). J. Therm. Sci. 29, 1097–1124. https://doi.org/10.1007/s11630-020-1365-4

Walker, G., von Backström, T.W., Gauché, P., 2012. A method of increasing collector aperture in linear Fresnel solar concentrators at high zenith angles, in: Southern African Solar Energy Conference, Stellenbosch, South Africa. pp. 1–9.

Walker, G.S., 2013. Development of a low cost linear Fresnel solar concentrator. M.Sc. Thesis, University of Stellenbosch, South Africa.

Wang, D., Zhou, H., 2019. Quantitative evaluation of the computational accuracy for the Monte Carlo calculation of radiative heat transfer. J. Quant. Spectrosc. Radiat. Transf. 226, 100–114. https://doi.org/10.1016/j.jqsrt.2019.01.001

Wang, G., Shen, F., Wang, F., Chen, Z., 2020a. Design and experimental study of a solar CPV system using CLFR concentrator. Sustain. Energy Technol. Assessments 40, 100751. https://doi.org/10.1016/j.seta.2020.100751

Wang, G., Wang, F., Shen, F., Chen, Z., Hu, P., 2019. Novel design and thermodynamic analysis of a solar concentration PV and thermal combined system based on compact linear Fresnel reflector. Energy 180, 133–148. https://doi.org/10.1016/j.energy.2019.05.082

Wang, G., Wang, F., Shen, F., Jiang, T., Chen, Z., Hu, P., 2020b. Experimental and optical performances of a solar CPV device using a linear Fresnel reflector concentrator. Renew. Energy 146, 2351–2361. https://doi.org/10.1016/j.renene.2019.08.090

Wang, Y., Potter, D., Asselineau, C.A., Corsi, C., Wagner, M., Blanco, M., Kim, J.S., Pye, J., 2018. Comparison of optical modelling tools for sunshape and surface slope error, in: AIP Conference Proceedings. https://doi.org/10.1063/1.5067222

Wang, Y., Potter, D., Asselineau, C.A., Corsi, C., Wagner, M., Caliot, C., Piaud, B., Blanco, M., Kim, J.S., Pye, J., 2020. Verification of optical modelling of sunshape and surface slope error for concentrating solar power systems. Sol. Energy 195, 461–474. https://doi.org/10.1016/j.solener.2019.11.035

Watts, N., Amann, M., Arnell, N., Ayeb-karlsson, S., Beagley, J., Belesova, K., Boykoff, M., Byass, P., Cai, W., Campbell-lendrum, D., Capstick, S., Chambers, J., Coleman, S., Dalin, C., Daly, M., Dasandi, N., Dasgupta, S., Davies, M., Napoli, C. Di, Dominguez-salas, P., Drummond, P., Dubrow, R., Ebi, K.L., Eckelman, M., Ekins, P., Escobar, L.E., Georgeson, L., Golder, S., Grace, D., Graham, H., Haggar, P., Hamilton, I., Hartinger, S., Hess, J., Maslin, M., Mcallister, L., Mcgushin, A., Mcmichael, C., Milner, J., Moradi-lakeh, M., Morrissey, K., Munzert, S., Murray, K.A., Neville, T., Nilsson, M., Sewe, M.O., Oreszczyn, T., Otto, M., Owfi, F., Pearman, O., Pencheon, D., Quinn, R., Rabbaniha, M., Robinson, E., Rocklöv, J., Romanello, M., Semenza, J.C., Sherman, J., Shi, L., Springmann, M., Tabatabaei, M., Taylor, J., Triñanes, J., Shumake-guillemot, J., Vu, B., Wilkinson, P., Winning, M., Gong, P., Montgomery, H., Costello, A., 2020. Review The 2020 report of The Lancet Countdown on health and climate change: responding to converging crises 6736. https://doi.org/10.1016/S0140-6736(20)32290-X

Wendelin, T., Dobos, A.P., Lewandowski, A., 2013. SolTRACE: A new optical modeling tool for concentrating solar optics, National Renewable Energy Laboratory. https://doi.org/10.1115/ISEC2003-44090

Winston, R., Minano, J., Benitez, P., 2005. Nonimaging optics. Elsevier.

World Nuclear Association, 2020. Where does our electricity come from? [WWW Document]. URL https://www.world-nuclear.org/nuclear-essentials/where-does-our-electricity-come-from.aspx

Yang, M., Zhu, Y., Taylor, R.A., 2018. End losses minimization of linear Fresnel reflectors with a simple, two-axis mechanical tracking system. Energy Convers. Manag. 161, 284–293. https://doi.org/10.1016/j.enconman.2018.01.082

Zhu, G., 2013. Development of an analytical optical method for linear fresnel collectors. Sol. Energy 94, 240–252. https://doi.org/10.1016/j.solener.2013.05.003

Zhu, G., Wendelin, T., Wagner, M.J., Kutscher, C., 2014. History, current state, and future of linear Fresnel concentrating solar collectors. Sol. Energy 103, 639–652. https://doi.org/10.1016/j.solener.2013.05.021

Zhu, J., Chen, Z., 2018. Optical design of compact linear Fresnel reflector systems. Sol. Energy Mater. Sol. Cells 176, 239–250. https://doi.org/10.1016/j.solmat.2017.12.016

Zhu, J., Huang, H., 2014. Design and thermal performances of semi-parabolic linear Fresnel reflector solar concentration collector. Energy Convers. Manag. 77, 733–737. https://doi.org/10.1016/j.enconman.2013.10.015

Zhu, Y., Jifu, S., Li, Y., Wang, L., Huang, Q., Xu, G., 2016. Design and experimental investigation of a stretched parabolic linear Fresnel reflector collecting system. Energy Convers. Manag. 126, 89–98. https://doi.org/10.1016/j.enconman.2016.07.073

Zhu, Y., Shi, J., Li, Y., Wang, L., Huang, Q., Xu, G., 2017. Design and thermal performances of a scalable linear Fresnel reflector solar system. Energy Convers. Manag. 146, 174–181. https://doi.org/10.1016/j.enconman.2017.05.031